

Diversity of Ganglion Cell Responses to Saccade-Like Image Shifts in the Primate Retina

Steffen Krüppel,^{1,2,3} Mohammad H. Khani,^{1,2,4} Dimokratis Karamanlis,^{1,2,4} Yunus C. Erol,^{1,2,4}  Sören J. Zapp,^{1,2} Matthias Mietsch,^{5,6}  Dario A. Protti,⁷ Fernando Rozenblit,^{1,2} and  Tim Gollisch^{1,2,3}

¹Department of Ophthalmology, University Medical Center Göttingen, 37075 Göttingen, Germany, ²Bernstein Center for Computational Neuroscience Göttingen, 37073 Göttingen, Germany, ³Cluster of Excellence “Multiscale Bioimaging: from Molecular Machines to Networks of Excitable Cells” (MBExC), University of Göttingen, 37075 Göttingen, Germany, ⁴International Max Planck Research School for Neurosciences, 37077 Göttingen, Germany, ⁵Laboratory Animal Science Unit, German Primate Center, 37077 Göttingen, Germany, ⁶German Center for Cardiovascular Research, 37075 Göttingen, Germany, and ⁷School of Medical Sciences (Neuroscience), The University of Sydney, Sydney 2006, New South Wales, Australia

Saccades are a fundamental part of natural vision. They interrupt fixations of the visual gaze and rapidly shift the image that falls onto the retina. These stimulus dynamics can cause activation or suppression of different retinal ganglion cells, but how they affect the encoding of visual information in different types of ganglion cells is largely unknown. Here, we recorded spiking responses to saccade-like shifts of luminance gratings from ganglion cells in isolated marmoset retinas and investigated how the activity depended on the combination of presaccadic and postsaccadic images. All identified cell types, On and Off parasol and midget cells, as well as a type of Large Off cells, displayed distinct response patterns, including particular sensitivity to either the presaccadic or the postsaccadic image or combinations thereof. In addition, Off parasol and Large Off cells, but not On cells, showed pronounced sensitivity to whether the image changed across the transition. Stimulus sensitivity of On cells could be explained based on their responses to step changes in light intensity, whereas Off cells, in particular, parasol and the Large Off cells, seem to be affected by additional interactions that are not triggered during simple light-intensity flashes. Together, our data show that ganglion cells in the primate retina are sensitive to different combinations of presaccadic and postsaccadic visual stimuli. This contributes to the functional diversity of the output signals of the retina and to asymmetries between On and Off pathways and provides evidence of signal processing beyond what is triggered by isolated steps in light intensity.

Key words: encoding; ganglion cells; model; primate retina; saccade; spikes

Significance Statement

Sudden eye movements (saccades) shift our direction of gaze, bringing new images in focus on our retinas. To study how retinal neurons deal with these rapid image transitions, we recorded spiking activity from ganglion cells, the output neurons of the retina, in isolated retinas of marmoset monkeys while shifting a projected image in a saccade-like fashion across the retina. We found that the cells do not just respond to the newly fixated image, but that different types of ganglion cells display different sensitivities to the presaccadic and postsaccadic stimulus patterns. Certain Off cells, for example, are sensitive to changes in the image across transitions, which contributes to differences between On and Off information channels and extends the range of encoded stimulus features.

Received Aug. 16, 2022; revised Apr. 12, 2023; accepted May 8, 2023.

Author contributions: S.K. and T.G. designed research; S.K., M.H.K., D.K., Y.C.E., S.J.Z., M.M., D.A.P., and F.R. performed research; S.K., M.H.K., D.K., Y.C.E., S.J.Z., and F.R. analyzed data; S.K. and T.G. wrote the paper.

This work was funded by the European Research Council under the European Union Horizon 2020 research and innovation program (Grant 724822), by Boehringer Ingelheim Fonds; and by the Deutsche Forschungsgemeinschaft (German Research Foundation) Projects 154113120 (SFB 889, project C01), 432680300 (SFB 1456, project B05), and 390729940 (Germany's Excellence Strategy—EXC 2067/1).

The authors declare no competing financial interests.

Correspondence should be addressed to Tim Gollisch at tim.gollisch@med.uni-goettingen.de.

<https://doi.org/10.1523/JNEUROSCI.1561-22.2023>

Copyright © 2023 the authors

Introduction

Research in visual neuroscience is often motivated by features of natural stimuli, like contrast, color, and dynamics of the visual environment. Fully natural stimuli, however, are so rich in features that elicited neural responses can often be difficult to interpret. It has thus proven useful to focus on a particular feature of natural stimuli and recreate it artificially in abstract form (Karamanlis et al., 2022), like changes in brightness investigated with uniform grayscale stimuli (Hartline, 1938), spatial structure at varying resolution with gratings (Enroth-Cugell and Robson,

1966), or small objects of interest with moving spots of light (Lettvin et al., 1959). A specific feature that dominates much of the dynamics of vision is given by saccades—rapid eye or body movements that shift the point of fixation and occur multiple times per second in humans (Yarbus, 1967). Saccades strongly structure the visual stimuli that fall onto the retina and thereby shape the neural signals sent from the eye to the rest of the brain.

Retinal ganglion cells can display diminished responsiveness during saccades or saccade-like image shifts, which is thought to contribute to saccadic suppression—the phenomenon of reduced visual perception around the time of saccades (Roska and Werblin, 2003; Wurtz, 2008; Idrees et al., 2020). However, psychophysical studies have found that saccade kinematics can be readjusted during the saccade if the target is moved at saccade onset (Gaveau et al., 2003), indicating that meaningful visual processing must occur during saccades. Indeed, suppression does not affect all retinal ganglion cells. Instead, cells can exhibit various responses to and during saccades (Noda and Adey, 1974; Amthor et al., 2005; Sivyer et al., 2019), and responses after saccade offset may furthermore be particularly informative about the newly fixated image (Segev et al., 2007; Krishnamoorthy et al., 2017). For macaque ganglion cells, a study found responses to natural scenes to be strongly shaped by the eye movement-like temporal structure of the stimulus (Schottdorf and Lee, 2021).

Little is known, however, about how the rapid succession of fixations and brief transitions affects the encoding of visual information, in particular for the primate retina. One hypothesis might be that a saccade acts like a reset, allowing a new, independent snapshot of the visual world after saccade offset. Retinal ganglion cells would then respond to the newly fixated image according to how strongly the encountered visual contrast activates their receptive fields. Yet, the offset of the previously fixated image also presents a potent stimulus just a few tens of milliseconds earlier. In principle, ganglion cell activity after a saccade may thus depend in a complex fashion on the combination of presaccadic and postsaccadic stimulus patterns and be additionally influenced by the image motion during the saccade.

Here, we investigate how primate retinal ganglion cell responses to saccade-like image shifts are shaped by the combination of presaccadic and postsaccadic stimulation of the receptive field. Based on multielectrode-array recordings of ganglion cells from the marmoset retina and functional identification of the major ganglion cell types, we find cell type-specific differences in the sensitivity to saccadic stimulus features. A model with nonlinear spatial stimulus integration and response properties derived from simple light-intensity flashes could partially capture these response characteristics. We conclude that saccades trigger cell type-specific signal-processing mechanisms that contribute to functional asymmetries between On and Off ganglion cells and broaden the scope of visual features encoded by the retina across saccades.

Materials and Methods

Experimental design and statistical analysis. We used retinas of four adult marmoset monkeys (*Callithrix jacchus*) of either sex (three male, one female; ages 4, 7, 10, and 15 years). Retinal tissue was obtained immediately after killing from animals used by other researchers, in accordance with national and institutional guidelines and as approved by the institutional animal care committee of the German Primate Center and by the responsible regional government office (Niedersächsisches Landesamt für Verbraucherschutz und Lebensmittelsicherheit, Permit 33.19-42 502-04-17/2496). For each of the four retinas, we obtained one multielectrode array recording of spiking activity from individual retinal

ganglion cells, yielding 80–600 cells per recording. No statistical method was used to predetermine sample size. To compare the performance of the investigated computational models across the population of recorded cells, *p*-values were calculated using the two-sided Wilcoxon signed-rank test implemented in the Python package SciPy.

Tissue preparation and electrophysiology. After enucleation, the eyes were dissected, and the cornea, lens, and vitreous humor were carefully removed to gain direct access to the retina. The tissue was then transferred into a light-tight chamber containing oxygenated (95% O₂ and 5% CO₂) Ames' medium (Sigma-Aldrich), supplemented with 6 mM D-glucose, and buffered with 22 mM NaHCO₃ to maintain a pH of 7.4. After 1–2 h of dark adaptation, the retina was dissected into smaller pieces. For each recording, a piece of peripheral retina was isolated from the pigment epithelium and transferred to a multielectrode array (MultiChannel Systems; either 60- or 252-electrode planar arrays; electrode diameter, 10 or 30 μm; minimum electrode spacing, 100 μm). The preparation was performed under infrared illumination with a stereomicroscope equipped with night vision goggles. During the recording, the retina was perfused with the oxygenated Ames' medium (4–5 ml/min), and the temperature of the recording chamber was kept constant around 33°C using an inline heater (model PH01, MultiChannel Systems) and a heating element below the array. The remaining retina tissue continued to be stored in the light-tight chamber and was constantly perfused with oxygenated Ames' medium for later recordings.

The multielectrode array signals were amplified, bandpass filtered (300 Hz to 5 kHz), and stored digitally at 25 kHz (60-electrode arrays) or 10 kHz (252-electrode arrays), using the software MC-Rack 4.6.2 (MultiChannel Systems). Spike sorting was performed with a modified version of the sorting software Kilosort (Pachitariu et al., 2016), available at <https://github.com/MouseLand/Kilosort> (original) and <https://github.com/dimokaramanlis/KiloSortMEA> (modified version). The output of Kilosort was visually inspected and manually curated with the software Phy2 (<https://github.com/cortex-lab/phy>). Only units with a well separated cluster of voltage traces and a clear refractory period were included for further analyses.

Visual stimulation. Visual stimuli were generated by custom-made software written in C++ and OpenGL and displayed on a gamma-corrected monochromatic white OLED monitor (eMagin) with a refresh rate of 60 Hz and 800 × 600 pixels. The stimuli were projected onto the retina using a telecentric lens (Edmund Optics), resulting in a pixel size of 7.5 × 7.5 μm on the retina. All stimuli used in this study had a mean light level of ~0.4, 0.9, or 3.3 mW/m², depending on the experiment, in the mesopic to low-photopic regime. We calculated the isomerization rates of the photoreceptors according to the formula presented in Lamb (1995), using peak sensitivities and collecting areas (cones, 0.37 μm²; rods, 1 μm²) available for marmoset and macaque (Travis et al., 1988; Schnapf et al., 1990; Tovée et al., 1992; Schneeweis and Schnapf, 1995). The obtained rates were as follows: rods: ~540, 1050, and 3670 isomerizations per photoreceptor per second, respectively; S-cones: 30, 50, and 190 isomerizations per photoreceptor per second; and M-cones: 250, 610, and 2110 isomerizations per photoreceptor per second. The same light level was also used for homogeneous illumination between stimuli. Before the start of an experiment, the projection of the stimulus screen was focused on the photoreceptor layer by visual inspection via a microscope.

Estimation of receptive fields, nonlinearities, and autocorrelations. To characterize the receptive fields of recorded cells and their autocorrelation functions, a spatiotemporal binary white noise stimulus on a checkerboard layout was presented. Stimulus pixels had a size of 60 by 60 μm or 37.5 by 37.5 μm on the retina. Each pixel was updated independently and pseudorandomly at the monitor refresh rate of 60 Hz to display either black or white (100% Michelson contrast). The stimulus consisted of an alternating sequence of 1500 frames (25 s) of independent, nonrepeating white noise and 300 frames (5 s) of a fixed, repeated white noise sequence. For the present study, only the independent white noise segments were used. The stimulus was presented for 30–40 min leading to ~100,000 frames of independent white noise.

Receptive fields were determined by first calculating the spatiotemporal spike-triggered average (STA) of the responses of a cell to the

independent white noise (Chichilnisky, 2001). We used a temporal window of 30 frames (0.5 s) for the STA. To separate the STA into a temporal and a spatial filter, we selected the element (pixel and time point) with the maximum absolute value in the STA after smoothing with a spatial Gaussian filter of 60 μm standard deviation (SD). The temporal filter was then defined as the time course of the selected pixel in the unsmoothed STA (normalized to unit Euclidean norm). The corresponding unsmoothed frame was used to obtain the spatial filter by fitting a two-dimensional Gaussian to it. The Gaussian fit is a customary way to reduce noise in the pixelwise representation of the STA, and most ganglion cell-receptive fields were well fitted by the elliptical Gaussian. The SD of the Gaussian was then reduced to 80% of the original to account for the observation that white noise stimuli activate the surround less strongly than flashed stimuli and therefore often overestimate the receptive field size relative to more flash-like stimuli with larger spatial structure (Wienbar and Schwartz, 2018). The reduced Gaussian function was normalized to a volume of unity and taken as an estimate of the receptive field, and the effective receptive field diameter was defined as the diameter of a circle with the same area as the 1.5 σ ellipse of this Gaussian function. Receptive field outlines were displayed as this 1.5 σ ellipse.

The layouts of receptive fields were also used to confirm the location of the recorded retina pieces as coming from the peripheral retina. To do so, we estimated the cell density of On and Off parasol cells (see below for cell type classification) by computing all nearest-neighbor distances of receptive field midpoints, finding the mode, and calculating the corresponding density of a hexagonal grid with that node distance. We found densities of 60–120 On parasol cells/ mm^2 and 80–160 Off parasol cells/ mm^2 , respectively, consistent with the peripheral retina according to literature values (Gomes et al., 2005).

To characterize the contrast–response relationship of a cell, we computed the nonlinearity of the cell as part of the linear–nonlinear model (Chichilnisky, 2001). This was done by computing the dot product of every frame in the white noise stimulus with the normalized spatial filter of the cell and convolving the resulting sequence with its normalized temporal filter to obtain a generator signal for each stimulus frame. To reduce noise, the length of the temporal filter was cut to 0.25 s, and only pixels within the smallest rectangular window still containing the 3.75 σ ellipse of the Gaussian were included in this computation. The generator signals were then binned into 10 bins with an equal number of data points, and the average spike count and generator signal were calculated for each bin.

Spike train autocorrelation functions were computed over 50 ms at a resolution of 0.04 ms (25 kHz recordings) or 0.1 ms (10 kHz recordings) from the responses to the white noise stimulus, smoothed with a Gaussian filter with an SD of 10 data points, and normalized to a sum of unity.

Classification of retinal ganglion cells. To be able to investigate whether different cell types play distinct roles during saccades, we first classified cells manually in a way similar to the procedure in the study by Field et al. (2007). For each recording, we computed the first two principal components of all temporal filters. We then constructed scatter plots of the projections of the temporal filters onto the first principal component against the projection onto the second principal component as well as against the effective receptive field diameter. The scatter plots yielded clustered groups of cells, corresponding to On and Off midget and parasol cells, respectively, and a fifth cell type that we here call Large Off cells. Many recorded cells could readily be assigned to one of the clusters based on these scatter plots. For cells that lay at the borders of clusters, assignment to a cluster was additionally based on examining the spike train autocorrelation function, the detailed shapes of the temporal filter and the nonlinearity, the pixel-wise display of the spatial component of the spike-triggered average, and the positioning of the receptive field relative to receptive fields of other cells in the nearby clusters. While the autocorrelation function and the estimated nonlinearity could often vary significantly within a cell type, the temporal filter and tiling of visual space by the receptive fields could be used more reliably to further distinguish cell types. Cells that could not be clearly assigned to one of the analyzed types were excluded from further analyses. In total, this led to 842 analyzed of 1172 recorded cells. The 330 excluded cells were,

presumably, mostly cells of types other than the five identified cell types or were too noisy to be classified.

Saccadic stimulus. To stimulate the retina with saccade-like image shifts, we used a stimulus based on rapid movements of a spatial square-wave grating. The grating had a Michelson contrast of 60% and a bar width of 90 μm on the retina. The stimulus mimicked an alternating sequence of fixations lasting 533 ms each and saccade-like transitions of 67 ms. During each fixation, the grating remained static at one of four equally spaced spatial phases, which are called Positions 1, 2, 3, and 4. The sequence of positions was chosen pseudorandomly. Transitions moved the grating from one position to the next by translating the grating by about two full grating periods, as previously used in the study by Krishnamoorthy et al. (2017). Note, however, that in our experiments, these motion transitions were depicted for only four monitor frames such that, because of aliasing, the screen did not show a smooth movement of the grating but rather a quick succession of various grating positions. For half of the transitions, chosen pseudorandomly, the transition was masked by a uniform gray screen at mean intensity of the grating. The saccadic stimulus was presented for 12–20 min, resulting in 1200–2000 transitions.

We analyzed the responses of each cell to the transitions according to the combination of grating position before the saccade, termed starting position, and the grating position after the saccade, termed target position. For each of the resulting 16 combinations of starting and target position, we collected the responses of the cell to calculate a 350-ms-long peristimulus time histogram (PSTH) with a bin size of 10 ms. For quantitative analyses of response amplitudes just after the onset of the transition and after the onset of the new fixation, we divided each PSTH into a first response window, ranging from 30 ms after onset of the transition until 10, 20, or 30 ms (selected manually for each experiment, depending on the response latencies observed in that experiment) after onset of the target position, and a second response window ranging from those 10–30 to 200 ms after the onset of the target position. Peak responses in each window were then determined after separately smoothing each corresponding PSTH segment with a Gaussian of 20 ms SD, using zero-padding.

The position of the boundary between the two response windows (10, 20, or 30 ms) was determined with the goal of separating the observed early and late response peaks for all cells that displayed such peaks (typically, On parasol and midget cells as well as Off parasol cells). We verified that response peak times for these cell types lay well within the considered response windows with sufficient distance from the selected boundaries. For each of these cell types and each response window, we examined the distribution of the time between response peak and selected boundary and found that the average was similar to or >2 SDs in each case. We also checked that for Off midget cells, which had more sustained responses with no obvious double-peak pattern, any response component that appeared to solely relate to the starting position was contained in the first response window. Such a response component is most easily identified in the transition that yields the strongest fixation offset and weakest fixation onset response; that is, the transition with equal starting and target position, both the opposite of the preferred target position. Large Off cells generally only showed a single response event, which occurred well inside the second response window.

We collected the detected peak firing rates in each of the two response windows in two 4×4 response matrices, one for each response window. These response matrices were then Fourier transformed (two-dimensional discrete Fourier transform), yielding two complex-valued matrices whose entries quantify the amplitudes and phases of different basic patterns in the response matrices. We took the absolute values of the matrix entries, thereby disregarding the phase and only keeping the amplitude of the patterns. From each transformed matrix, we extracted the three entries (0, 1), (1, 0), and (3, 1), which correspond to specific sensitivities (to starting position, to target position, and to change across the transition), as described in the main text. These three entries were combined in a three-dimensional vector, yielding two vectors for each cell that needed to be normalized to make them comparable across cells. This was done by comparing the Frobenius norms of the two Fourier-transformed response matrices and dividing both vectors by the larger

one. Intuitively, this relates each specific response modulation pattern to the total response modulation in the response window with the stronger modulations. After having observed that three of the six entries of the two vectors are almost always close to zero, the remaining three values were combined into a final sensitivity vector, as follows: the (0, 1) component (i.e., start sensitivity) of the vector of the first response window; and the (1, 0) and (3, 1) components (i.e., target and change sensitivity) of the vector of the second response window.

Flashed gratings. As a means to judge the responses of cells to individually flashed gratings, we used a stimulus that was designed to test the responses of cells to reversing gratings. The grating stimulus started with 1 s of full-field mean light intensity gray, after which a square-wave grating with 100% Michelson contrast was presented. Every 0.2 s, the polarity of the grating was reversed, with 24 reversals in total. After the 25th grating presentation, the stimulus returned to gray for 1 s before the next reversing grating started. The grating size cycled through a list of bar widths of 7.5, 15, 30, 60, 120, 240, 480, and 6000 μm (full-field) in this order, and for each of those bar widths a specified number of different spatial phases was tested: 1, 1, 2, 2, 4, 4, 8, and 1, respectively. For example, the 30 μm grating was presented first at a relative spatial phase shift of 0°, then at a shift of 90°. The entire paradigm was shown twice, taking ~ 5 min in total.

PSTHs for the onset and offset of the grating were calculated with a bin size of 10 ms for each grating size regardless of spatial phase. To display individual response traces, we calculated the PSTHs from 0.3 s before onset until 0.4 s after onset, and from 0.4 s before offset until 0.3 s after offset, respectively. For population analyses, only the 0.2 s after onset/offset were considered. In this time window, the average firing rate was computed as a measure of response strength for the grating onset and offset (rather than using the peak firing rate, which is more strongly affected by noise from the small number of trials). Furthermore, to compare with the relative sensitivities during the saccade stimulus, since the 90 μm bar width of the saccade stimulus was not available in the reversing-gratings data, the strengths for 60 and 120 μm were averaged for grating onset and offset, respectively. Finally, we computed the relative strengths of onset versus offset response and the relative sensitivity to target versus starting position according to $(a - b)/(a + b)$, where a and b are the two response strengths (onset and offset) or sensitivities (target and start).

To estimate the response quality of the cells (see subsection Cell selection), we also calculated PSTHs for the reversing part of the stimulus. PSTHs were calculated for a duration of one reversing cycle (0.4 s) with a bin size of 10 ms, separately for each grating size and grating phase, disregarding the first half cycle of the grating to reduce onset effects.

Responses to brightness steps. We used the responses of ganglion cells to full-field steps in light intensity as a basis for modeling their responses to the saccadic stimulus. The light intensity steps lasted 0.5 s, going alternately to white (+100% Weber contrast) and black (−100% Weber contrast), separated by 1.5 s of gray mean intensity illumination. This stimulus was repeated for 30–90 cycles, taking a total of 2–6 min. PSTHs were computed with a bin size of 10 ms both for the entire cycle duration for display in the figures, and for a time window of 400 ms following each of the four changes in light intensity for the modeling of responses to the saccadic stimulus (see below).

Modeling. We compared the ability of two computational models to predict ganglion cell responses to the saccadic stimulus based on the responses of a cell to the brightness steps. For these analyses, the transition period was modeled as homogeneous gray illumination at mean light intensity, based on the observation that measured responses did not differ much between such masked transitions and transitions with shifting grating position.

Both models use a weighted summation of the firing-rate profiles measured under brightness steps. The two models only differed in whether contrast signals over the receptive field were integrated linearly or nonlinearly when computing the weights. For the linear model, we first computed the net change in visual contrast over the receptive field for each transition in the saccade stimulus and used this as a weight for the corresponding response trace as measured under the brightness steps to arrive at the model prediction. Conversely, for the nonlinear model,

we calculated a firing-rate prediction for each pixel individually according to its own contrast change, and only afterward averaged over the receptive field, thus preventing the direct cancellation of activity by simultaneous brightening and darkening in the different parts of the receptive field.

Concretely, the two model predictions $R_{\text{linear}}(t)$ and $R_{\text{nonlinear}}(t)$ of a cell were computed from the responses of the cell $R_{x \rightarrow y}(t)$ under brightness steps, where $x \rightarrow y$ stands for the different transitions white \rightarrow gray ($w \rightarrow g$), black \rightarrow gray ($b \rightarrow g$), gray \rightarrow white ($g \rightarrow w$), and gray \rightarrow black ($g \rightarrow b$). For a given transition from the presaccadic stimulus S_{pre} to the postsaccadic stimulus S_{post} , we used the following:

$$R_{\text{linear}}(t) = \sum_{\text{all } x \rightarrow y} N(\bar{W} \cdot \bar{S}_n \cdot \sigma_{x \rightarrow y}) \cdot R_{x \rightarrow y}(t - d_n),$$

and

$$R_{\text{nonlinear}}(t) = \sum_{\text{all } x \rightarrow y} \bar{W} \cdot N(\bar{S}_n \cdot \sigma_{x \rightarrow y}) \cdot R_{x \rightarrow y}(t - d_n).$$

Here, $N(\cdot)$ is a thresholding function, setting negative inputs to zero, and \bar{W} is the (Gaussian) receptive field of the cell (positive also for Off cells), evaluated at the pixel centers and correspondingly denoted as a vector. \bar{S}_n stands for the appropriate pixel-wise stimulus, \bar{S}_{pre} for the presaccadic image used for $w \rightarrow g$ and $b \rightarrow g$, and \bar{S}_{post} for the postsaccadic image used for $g \rightarrow w$ and $g \rightarrow b$. The elements of the \bar{S}_n are -0.6 and 0.6 for dark and bright pixels, respectively, denoting the contrast values that were used in the saccadic stimulus. The time delay d_n is used to shift the responses corresponding to the occurrence of S_{post} by the transition duration, hence $d_{\text{post}} = 67$ ms and $d_{\text{pre}} = 0$ ms. The scalar factor $\sigma_{x \rightarrow y}$ is used to switch the sign of the stimulus elements when the contribution of a step from or to black is considered; hence, $\sigma_{x \rightarrow y} = -1$ for $b \rightarrow g$ and for $g \rightarrow b$, and 1 otherwise. For the $R_{x \rightarrow y}(t)$, we used the 400-ms-long PSTHs of the cell after the full-field brightness step from x to y (as calculated in the subsection Responses to brightness steps) and zero padded them for time points outside of the 400 ms window.

Finally, for comparison with measured responses to the saccade stimulus, we allowed for a constant latency shift that is applied in the same way to the firing rate predictions for all 16 transitions. This aims at accounting for the overall faster responses under brightness steps, owing to the higher contrast of this stimulus compared with the saccade stimulus. We fitted the latency shift for each cell by selecting the shift in the range of 0–50 ms with the maximal Pearson correlation between the data and the prediction. For most cells, the latency shift was < 30 ms. Predictions were calculated for a 350 ms window starting at the onset of the transition, which is the same duration as the PSTHs calculated for the saccadic stimulus. For figures showing predicted responses, we jointly scaled the predictions for the 16 transitions to the same peak value as in the corresponding data from that cell, again to account for differences in applied overall contrast.

We used two measures to evaluate the model performance. First, we compared the response matrices calculated from the predicted responses with the experimental response matrices of the cell using a modified coefficient of determination. The modeled response matrices were scaled to the same mean as the experimental ones to accommodate for the different contrasts. The modified coefficient of determination between one pair of experimental and modeled response matrices was then calculated as follows:

$$R^2 = 1 - \frac{\sum_{i,j} (m_{i,j}^{\text{data}} - m_{i,j}^{\text{model}})^2}{\sum_{i,j} (m_{i,j}^{\text{data}})^2},$$

where $m_{i,j}$ are the entries of the response matrix of the experimental data or of the prediction, respectively. This modified coefficient of determination corresponds to substituting the mean of the response matrix of the data in the denominator of the regular coefficient of determination with zero. This effectively uses the total response strength as a signal rather

than the deviation from the mean and avoids the fact that the denominator goes to zero for cells that respond equally to all transitions.

Furthermore, we used the Euclidean distance in the three-dimensional sensitivity vector space as a measure for model performance. The distance was computed between the sensitivity vector as calculated from the model predictions and the sensitivity vector of the experimental data. A low distance indicates that the coding properties have been reproduced well by the model.

Cell selection. In addition to excluding cells that could not be matched to one of the five analyzed cell types as noted above, we excluded cells from further analyses that responded unreliably during the relevant stimuli. To measure the reliability of a cell during the saccadic stimulus, we first split its responses into odd and even trials and calculated PSTHs individually. We then linked the 16 PSTHs of different starting and target position combinations together to generate a single PSTH for all odd trials and a single PSTH for all even trials. Next, we computed the coefficient of determination R^2 between the odd PSTH as data and the even PSTH as prediction, and vice versa, and averaged these two values (Karamanlis and Gollisch, 2021). Any cell with an average $R^2 \leq 0.2$ for the saccadic stimulus was excluded from all analyses using that stimulus. In total, we analyzed the saccade responses of 166 On parasol, 41 On midget, 182 Off parasol, 51 Off midget, and 13 Large Off cells from four experiments.

For the analyses of the flashed-grating responses, we calculated the reliability similarly by computing PSTHs of the reversing part of the stimulus separately for the first and second presentations of the stimulus, linking the PSTHs of the different grating sizes and phases together, and computing the coefficient of determination R^2 between the two PSTHs as above. For this part of the analysis, we considered all cells with an averaged $R^2 > 0.2$ for the reversing-gratings stimulus. This led to 151 On parasol, 49 On midget, 154 Off parasol, 40 Off midget, and 6 Large Off cells for the flashed-grating analysis.

For modeling responses to the saccadic stimulus, cells had to be sufficiently reliable during both the saccadic as well as the full-field brightness steps stimulus. For calculating the reliability during the full-field brightness steps, we proceeded similarly as above, but only considered the 400 ms after any brightness change to exclude long periods without changes in the stimulus. Again, we determined all cells with an averaged $R^2 > 0.2$ to be reliable enough, leading to 122 On parasol, 25 On midget, 144 Off parasol, 37 Off midget, and 11 Large Off cells for the modeling part of our analysis.

Data availability. The spike train data recorded for this work have been made publicly available at https://gin.g-node.org/gollischlab/Krueppel_et_al_2023_Marmoset_RGC_spiketrains_to_saccadic_shifts (DOI: 10.12751/g-node.th1j).

Results

Stimulus and analysis

Saccades form rapid transitions between fixated images, and elicited responses in neurons of the visual system may be influenced by the presaccadic image, the postsaccadic image, and the transition in between. To investigate the coding properties of ganglion cells in the primate retina under saccade-like image transitions, we recorded ganglion cell spiking activity in isolated marmoset retinas with multielectrode arrays while projecting a saccade-like stimulus onto the photoreceptors. To systematically probe transitions between different illumination patterns inside the receptive fields of different ganglion cells, we chose a square-wave luminance grating with a bar width of 90 μm as the spatial layout of the stimulus. Taking into account the size of the marmoset eye (Troilo et al., 1993), this corresponds to $\sim 0.9^\circ$ visual angle or, for example, a 10-cm-thick tree branch at a distance of ~ 6 m.

To mimic the sequential order of fixations and saccades, the grating remained stationary for a fixation period of 533 ms at one of four equally spaced positions, which we call Position 1–4,

before being shifted rapidly within 67 ms to a new position to start the next cycle of fixation and transition (Fig. 1A). In half of the transitions, the shift itself was masked by a gray screen at the mean light intensity of the grating to probe for effects of visual stimulation during the transition. The order of fixation positions and the occurrence of the gray-screen mask were randomized. Altogether, there were 16 possible combinations of grating positions before (“starting position”) and after (“target position”) a transition, and each combination was presented with transitions by grating motion as well as by homogeneous illumination.

We observed that ganglion cell responses could depend on the grating position both before and after the transition. Some of the different response patterns and their dependencies on starting and target positions are exemplified by the three sample cells displayed in Figure 1B. Cell 1 responded strongly after transitions from Position 3 to Position 2 as well as from Position 1 to Position 2, but not for transitions from Position 3 to Position 4, suggesting a preference for a specific target position, namely here Position 2. When comparing firing rate profiles for transitions via motion and via a gray screen, on the other hand, nearly identical responses were found for each individual combination of starting and target image. This was also the case for the two other sample cells of Figure 1 as well as for the entire population of ganglion cells, except for a small latency effect in some cells (e.g., Cells 2 and 3).

For a quantitative comparison of the responses under transitions via motion and via a gray screen, we computed a normalized coefficient of determination R^2 between the two responses (Fig. 1D). Most values lay near unity, corresponding to nearly identical response profiles under the two conditions, and values smaller than unity could generally be traced back to relative temporal shifts of the responses. These small differences in response kinetics, however, did not play a role for our analysis of response strength and sensitivity to the presaccadic and postsaccadic images. We therefore generally pooled responses from motion and gray-screen transitions for further analyses, but also confirmed that the analysis of response types held independently for each of the two transition types (see below).

To visualize the response characteristics more systematically, we computed the PSTHs for all 16 combinations of starting and target positions and displayed them in a matrix-like fashion (Fig. 1C). In this depiction, it becomes immediately apparent that Cell 1 responded strongly when the target grating position was Position 2, but not for other targets, and that the response was only slightly modulated by the starting position. Thus, this cell is sensitive mostly to the postsaccadic image, in this particular case the image that corresponds to the grating at Position 2. Note that the relevant observation here is that there is a preferred target position, but not which particular position it is. For the same cell but with a translated receptive field position or for phase-shifted versions of the displayed gratings, the preferred target position might be different, but responses should still primarily depend on which target position was reached.

Other ganglion cells, like Cell 2, could display two distinct response peaks, one during the transition itself and one after the onset of the new fixation. For this cell, both peaks occurred when the grating switched from Position 3 to Position 1, but other sample transitions with a different starting or target position elicited only one or the other (Fig. 1B, center). The matrix-like display of all 16 firing rate profiles (Fig. 1C, center) reveals that the first peak was sensitive to the starting position, occurring systematically for Positions 2 and 3, whereas the second peak depended

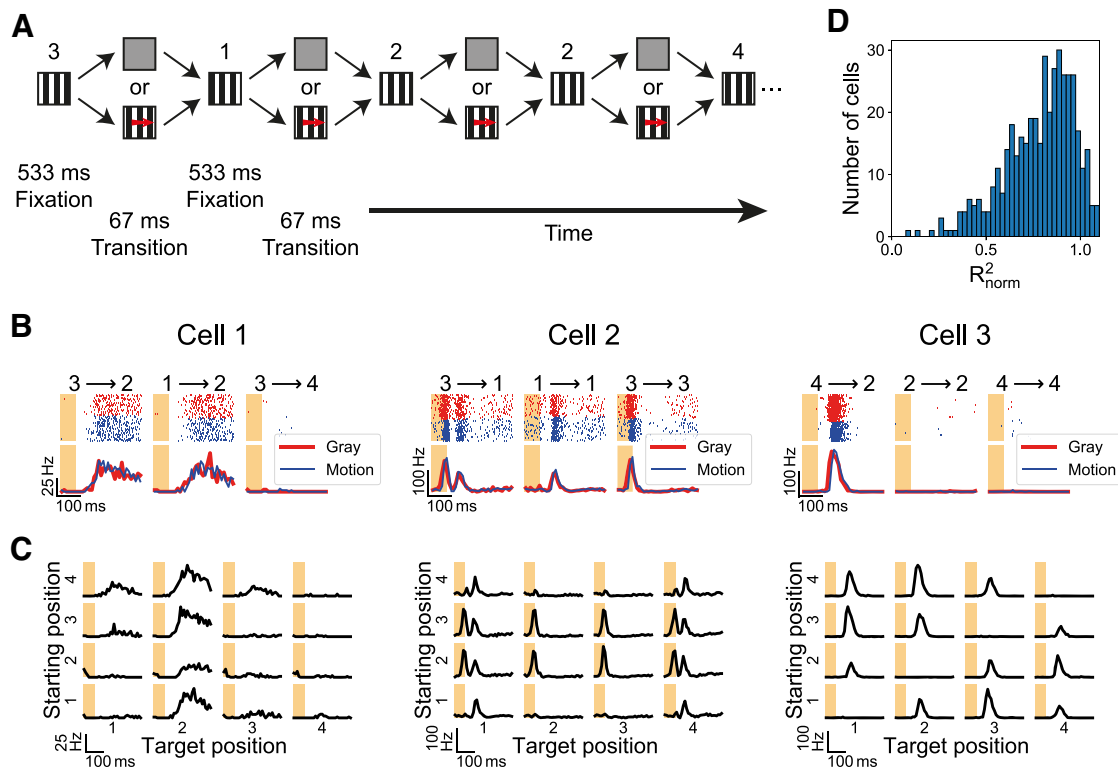


Figure 1. Sample ganglion cell responses to saccade-like grating shifts. **A**, Schematic representation of the stimulus, consisting of a sequence of 533 ms fixations of a square-wave grating at one of four possible positions (spatial phases) and brief transitions of 67 ms. The transition either occurred via a rapid motion of the grating or via a gray-screen mask at mean luminance. The sequence of fixation positions and the type of transition were randomized. **B**, Responses of three sample ganglion cells to different combinations of grating position before and after the transition. Top row, Raster plots for both gray (red) and motion (blue) transitions. Bottom row, Corresponding PSTHs. Shaded areas mark the transition periods. **C**, PSTHs of the sample cells for all 16 possible combinations of grating positions before the transition (starting position) and after the transition (target position). Here, responses to gray-screen and motion transitions were pooled. **D**, Similarity of responses to gray and motion transitions for all cells included in the analysis. The similarity measure R_{norm}^2 was calculated as the modified coefficient of determination between responses to gray and to motion, normalized by the corresponding coefficient for odd versus even trials (independent of the transition type). Nearly all R_{norm}^2 values are >0.5 , indicating high similarity between the responses to gray and motion transition.

on the target position and was elicited by Positions 1 and 4. Note that because of the cyclical nature of the grating, Positions 1 and 4 are neighboring, just like Positions 2 and 3 are.

For some ganglion cells, responses to the saccadic stimulus depended more intricately on the combination of presaccadic and postsaccadic images. Cell 3, for example, exhibited increased activity when the grating changed from Position 4 to Position 2, but neither the starting nor the target position alone were sufficient to evoke a strong response if there was no change in the grating position across the transition (Fig. 1*B*, right). Indeed, none of the starting or target positions by itself were sufficient to evoke a response of Cell 3, because starting and target position had to differ to trigger the cell (Fig. 1*C*, right). Thus, this cell was sensitive to a change in the grating position, but invariant to the specific starting and target positions of the transition.

To systematically compare these response patterns for different types of ganglion cells, we sought a reduced, quantitative description that still captured the dependencies of the responses on the starting position, on the target position, and on whether there was a change of the position. To take the distinct early and late responses of some cells into account (Fig. 1, Cell 2), we analyzed the peak firing rates in two response windows, the first from 30 ms after transition onset to 10–30 ms (depending on the experiment) after the onset of the new fixation, and the second from 10 to 30 ms until 200 ms after the onset of the new fixation (Fig. 2*A*).

To systematically analyze the dependence of the responses in these two temporal windows on the combination of starting and

target position of the grating, we collected the peak firing rates of each window in a 4×4 matrix, corresponding to the 4×4 transitions from starting to target position (Fig. 2*B*). The structure of these two response matrices contains information about the sensitivity of the cell to specific grating positions. For example, the first response matrix of Cell 2 from Figure 1, displayed in Figure 2*B* (left), contains horizontal stripes, demonstrating its sensitivity to specific starting positions (here Positions 2 and 3). The vertical stripes in the response matrix for the second time window (Fig. 2*B*, right), on the other hand, correspond to sensitivity to specific target positions.

The occurrence of stripes in the response matrices thus denotes the stimulus sensitivity during the selected response window. The specific position of the stripes, however, merely depends on the location of the receptive field of the cell relative to the bars of the grating. For example, Position 2 of the grating presumably brought an increase in preferred contrast to the receptive field of Cell 1 in Figure 1, but if the receptive field of that cell had been displaced by a quarter grating period in the right direction, the same response peak would have occurred for Position 3 instead.

Therefore, to make the analysis invariant to the receptive field position, we applied a two-dimensional Fourier transformation to the response matrices and only considered the amplitudes of the Fourier components. This yielded a 4×4 matrix for each of the two time windows (Fig. 2*C*). The Fourier component amplitudes in these matrices capture how strongly different

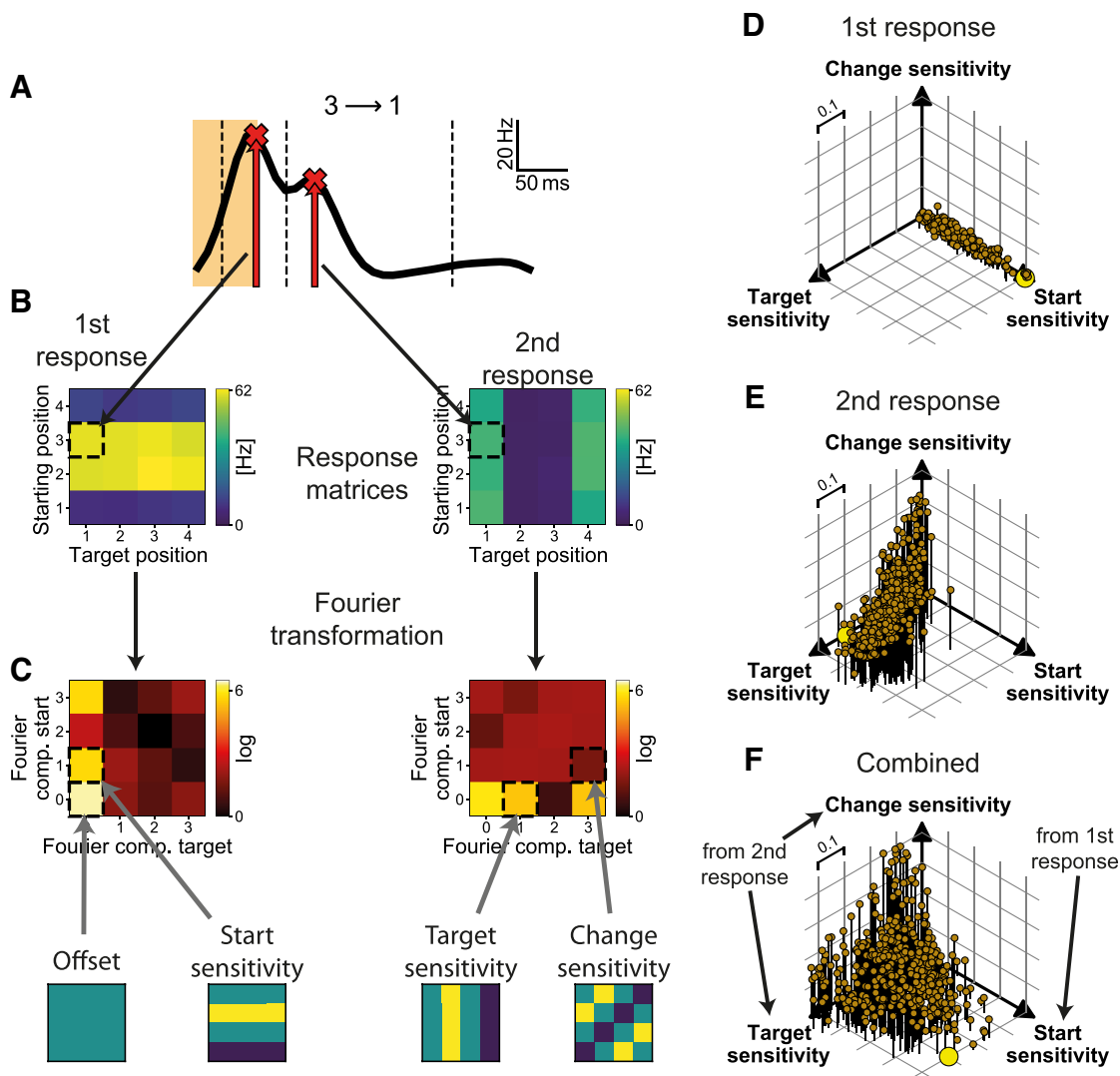


Figure 2. Analysis of ganglion cell sensitivity. **A**, PSTH of a sample cell (Fig. 1, Cell 2) for the transition between Position 3 and Position 1, smoothed by a Gaussian filter. (In the quantitative analysis, the two response windows were smoothed separately.) Dashed vertical lines mark the boundaries of the first and second response windows. For each response window, the peak response is identified as depicted by the red crosses and arrows. **B**, The response matrices contain the peak response during the first window (left) and second window (right) for all combinations of starting and target position, depicted here in a color-coded fashion with brighter colors denoting stronger responses. The dashed squares indicate the entries that correspond to the sample PSTH shown in **A**. **C**, Fourier transformations of the response matrices. The entries of the transformed matrices quantify patterns in the response matrices. Entries that are highlighted by dashed squares correspond to relevant patterns in the response matrix, which are depicted schematically below the Fourier transformed matrices. For the sample cell, the yellow (0, 1) entry of the first and the yellow (1, 0) entry of the second Fourier transformed response matrix reflect the start and target sensitivity of the cell. **D**, Scatter plot of the start, target, and change sensitivity of the first response window for each cell. The large yellow data point marks the sample cell from **A–C**. **E**, Same for the sensitivity of the second response window. **F**, Elements of the final sensitivity vector for each cell, obtained by combining the start sensitivity of the first response window and the target and change sensitivity of the second response window.

wave-like (or stripe-like) patterns are represented in the response matrices, such as stripes along the horizontal, vertical, or diagonal directions. Information about the exact positions of these stripes, on the other hand, is contained in the phases of the Fourier components, which were discarded in our analysis to assess the structure of the response matrices independent of relative position (or phase).

Three entries of the Fourier transformed response matrices are of particular interest as they correspond to the aforementioned sensitivities to starting position, target position, and change of position (Fig. 2C). Simple patterns with single horizontal and vertical stripes in the response matrices, for example, corresponding to sensitivity to the starting and target position, are captured by the (0, 1) and the (1, 0) entry, respectively, of the Fourier transform regardless of the exact preferred position; patterns with diagonal stripes, on the other hand, are typically

reflected in the (3, 1) component. These relevant entries are pointed out by arrows in Figure 2C, and corresponding insets show stereotypical response matrix patterns represented by these components.

The entries (0, 2), (2, 0), and (2, 2) would correspond to higher harmonics in the sensitivity matrix (e.g., high activity for Positions 1 and 3, but low activity for Positions 2 and 4), and the (1, 1) component to activity patterns along the other diagonal in the response matrix, from top left to bottom right. As expected, such patterns are generally not observed in our data, and the corresponding Fourier components are always near zero. The remaining components either capture the mean activity, namely the (0, 0) component, or are redundant copies of components already discussed. Thus, for each response window, there are three entries of the Fourier transformed response matrices that capture the basic sensitivity pattern of the cell, as follows: the (0, 1), the

(1, 0), and the (3, 1) components, which correspond to the aforementioned sensitivities to starting position, target position, and change of position.

As an example, the cell of Figure 2 exhibited a large (0, 1) Fourier component for the first time window and a large (1, 0) component for the second time window, reflecting its sensitivity to starting and target position in the first and second response window, respectively. Cell 3 from Figure 1, on the other hand, had a diagonal stripe in its second response matrix, reflected by a large (3, 1) entry (data not shown). Note that, in the case of this Cell 3, the large (3, 1) Fourier component was caused by decreased activity along the diagonal of equal starting and target position. Such sensitivity to image recurrence has indeed been described for certain ganglion cells of the mouse retina (Krishnamoorthy et al., 2017). For the present datasets from the marmoset, however, we did not find any image-recurrence-sensitive cells. A strong (3, 1) entry in our data always corresponded to a decrease of responses along the diagonal and thus a response sensitivity to a change of the grating position. Finally, for some cells, none of the three entries described above contained a large value. In such a case, the cell either did not respond at all during the corresponding time window or responded indifferently to all transitions with no dependence on the starting or target position or any combination of the two.

To compare the sensitivities to presaccadic and postsaccadic images and combinations thereof across cells, we combined the three relevant entries of each Fourier transformed response matrix [(0, 1), (1, 0), and (3, 1)] into a three-component vector and normalized it (see Materials and Methods). For each response time window, its elements thus characterize the sensitivity of a given cell to the starting position, to the target position, and to change in the fixated stimulus pattern across the saccade. Examining this vector for the first response window for each ganglion cell (Fig. 2D) shows that this response window was generally only sensitive to the starting position, as the other two Fourier components for target position and change sensitivity were always near zero. This was expected, as the first response occurs too early to be affected by the new fixation and is thus mostly elicited by the offset of the starting position grating. The second response, on the other hand, was dominated by the components corresponding to sensitivity to the target position and to change, with considerable differences in the magnitude of these two components between individual cells, but with generally little sensitivity to the starting position alone (Fig. 2E). Thus, this response component is typically affected by the target position of the grating and by combinations of the starting position with the target position, consistent with its occurrence several tens of milliseconds after the onset of the new fixation.

To jointly analyze the most relevant patterns of stimulus sensitivities during the first and second response window, we thus combined the sensitivity for the starting position of the first response with the target and change sensitivities of the second

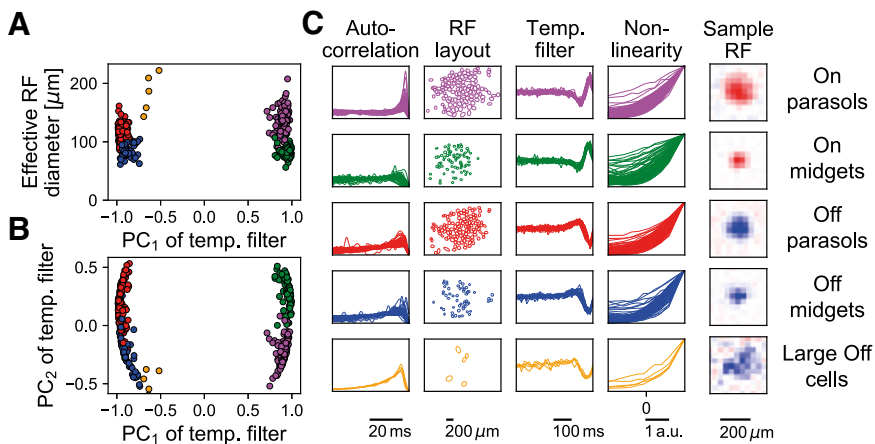


Figure 3. Classification of retinal ganglion cells of a sample experiment. **A**, Scatter plot of the effective receptive field diameter versus the projection onto the first principal component of the temporal filter for all classified cells (magenta, On parasol cells; green, On midglet cells; red, Off parasol cells; blue, Off midglet cells; orange, Large Off cells). **B**, Same as **A**, but for second principal component versus first principal component of the temporal filter. **C**, Autocorrelation functions, receptive field layouts (1.5- σ ellipses of receptive field Gaussians; distant cells excluded), temporal filters, nonlinearities (scaled to the same maximum) of all classified cells, and a sample spatial filter, grouped by cell type.

response to obtain a final three-component vector, which we call the sensitivity vector. The sensitivity vector describes the most pronounced response properties of a ganglion cell under our saccade stimulus (Fig. 2F). For example, the sensitivity vector for the sample cell of Figure 2A–C (Fig. 2D–F, large yellow dot) has large sensitivity values for the starting and the target position, but not for the change of position, reflecting the horizontal and vertical stripes in the response matrices of Figure 2B and the lack of a diagonal structure.

As the sensitivity vector provides a general characterization of the sensitivity of a cell to pre- and post-transition image information, we used it to reconfirm that there was no significant difference between motion and gray-screen transitions. For each cell, we calculated the sensitivity vector separately for each transition type and assessed their difference as the Euclidean distance between the two sensitivity vectors, normalized by the Euclidean norm of the standard sensitivity vector for the cell. This can be viewed as a relative deviation of the sensitivity profile under motion versus gray-screen transitions, and the small average (mean \pm SD across all analyzed cells) value of 0.16 ± 0.13 indicated that sensitivity profiles varied little with transition type. In fact, the relative deviations are consistent with noise, as a corresponding analysis that split the data in half (regardless of the transition type) yielded comparable relative deviations of the sensitivity vectors of 0.12 ± 0.11 (mean \pm SD), corroborating that the transition type has little influence on the sensitivity profile with respect to pre- and post-transition images.

Responses of different cell classes

We next asked whether the observed differences in response sensitivities were connected to the different types of ganglion cells. To investigate this question, we first classified cells according to standard response characteristics measured under spatiotemporal white noise stimulation. Specifically, we measured the spatial receptive fields and temporal filters of the cells via the spatiotemporal spike-triggered average as well as the output nonlinearities and spike autocorrelations of the cells (Fig. 3; see Materials and Methods). Five distinct classes could be readily identified,

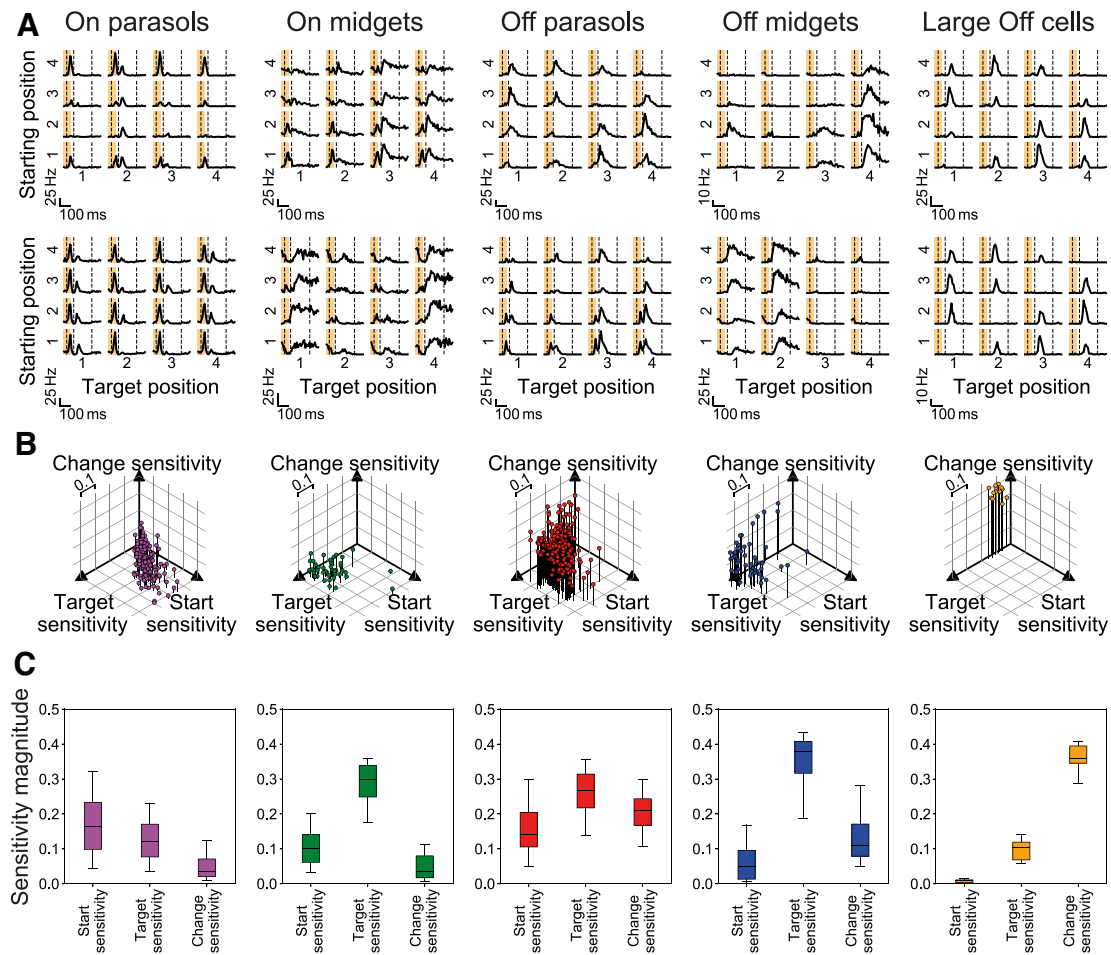


Figure 4. Coding properties of ganglion cell types. **A**, PSTHs of different sample cells, showing the responses of the cells to all 16 combinations of starting and target position. Shaded regions denote the transition period and dashed vertical lines mark the borders of the response windows used for analysis. **B**, Sensitivity vectors of all cells of the five distinguished cell types. **C**, Boxplots of the distributions of sensitivity measures (entries of the sensitivity vector) for each of the five cell types. Boxes denote the central 50% of data points (i.e., from 25% to 75%), whiskers the central 90% (i.e., from 5% to 95%), and horizontal lines inside the boxes the medians.

including the standard types of On and Off parasol cells as well as midget cells. On and Off parasol cells displayed fast, biphasic temporal filters and extensive receptive field tiling. On and Off midget cells had slower filters and smaller receptive fields. Here, however, tiling could only partially be observed, owing to the limited number of recorded cells. The reason for the unequal sampling of midget and parasol cells likely lies in a recording bias of the multielectrode arrays. The fairly wide spacing of electrodes and potential differences in signal-to-noise ratio of recorded spikes may result in more misses and rejections during spike sorting for the smaller midget cells. In addition, some midget cells may not have responded well to the applied stimuli, because of their relatively strong receptive field surround. In addition to these four major primate ganglion cell types, we also identified a fifth type, an Off cell with slow temporal filters and large receptive fields. We here refer to this type as Large Off cells.

We found that the identified major cell types exhibited distinct characteristic responses to the saccadic stimulus. Figure 4A shows representative response profiles, which illustrate the differences in response patterns between the cell types. Many On parasol cells had two separate response components, a first response sensitive to the starting position and a second response sensitive to the target position. For example, the first On parasol cell in Figure 4A (left column, top) displayed an early response

peak if the starting position was 4 (weaker if it was 1 or 3) and a later response peak if the target position was 2. Other On parasol cells did not show a clear preference for specific starting or target positions and instead responded rather indifferently (Fig. 4A, left column, bottom example). The sensitivity vectors of all On parasol cells show that there was a continuum between these two response types with indifferent cells lying closer to the origin (Fig. 4B, left column).

Figure 4C displays boxplots of the distributions over cells of the different sensitivity components. For On parasol cells (left column), this confirmed that the cells were mostly sensitive to the starting position and (somewhat less) to the target position. Change sensitivity only played a subordinate role. In one experiment, though, we also found a few On parasol cells whose second response did not seem to be sensitive to the target position but rather to the change of position.

Similar to On parasol cells, On midget cells (Fig. 4A, second column) also showed a first response sensitive to the starting position and a second response sensitive to the target position. In contrast to their parasol counterparts, however, the responses of On midget cells were dominated by the second response peak, which was more pronounced and sustained than the first. This shifts the sensitivity balance toward the target position (Fig. 4B,C).

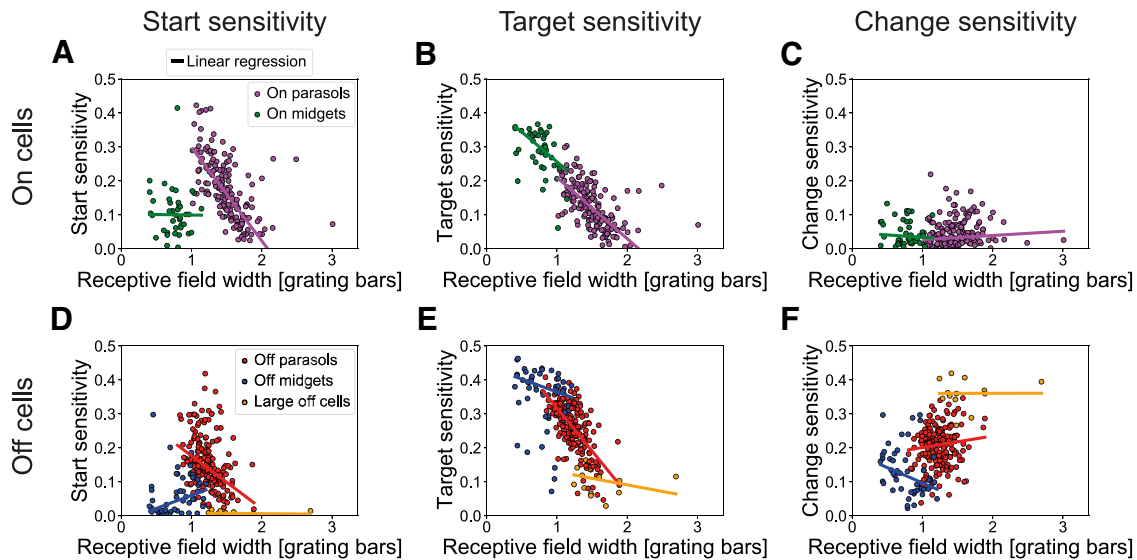


Figure 5. Dependence of stimulus sensitivities on receptive field size. **A**, Sensitivity to the starting position versus width of the receptive field for all On cells. Receptive field width was defined as the extent in x -direction (perpendicular to the grating) of the $1.5\text{-}\sigma$ ellipse of the receptive field Gaussian and given relative to the size of a grating bar. Circles represent individual cells, and solid lines are robust linear regressions for each cell type using the Theil-Sen estimator. **B**, Same as in **A**, but for sensitivity to the target position. **C**, Same as in **A**, but for sensitivity to change. **D–F**, Same as in **A–C**, but for Off cells.

For Off parasol cells, the most striking response feature was that many cells were sensitive to a change of the grating position across the transition. This is evident from the reduced responses during the second response window on the diagonal of equal starting and target position in the matrix representation of the PSTHs (Fig. 4A, third column) as well as from the large change sensitivity component of the sensitivity vectors (Fig. 4B,C). In addition, however, there often was also considerable sensitivity to the specific starting and target positions in the first and second response, respectively.

Off midget cells were mainly sensitive to the target position. Both examples in Figure 4A (fourth column) show cells that responded only to the occurrence of one or two specific target positions with only some modulation by the starting position. The moderate amount of modulation by the starting position was such that responses to a recurrence of the same grating position were reduced. This mild change sensitivity is also revealed by the sensitivity vectors (Fig. 4B,C). Overall, however, Off midget cell responses were dominated by their target sensitivity, which they displayed more strongly than any of the other cell types.

For the Large Off cells, the striking feature was their pronounced sensitivity to the change of the grating position (Fig. 4A, right column) with essentially no sensitivity to the specific starting or target position (Fig. 4B,C). These cells generally showed no activity during the first response window and transient responses during the second whenever starting and target position differed.

There are thus systematic differences in the sensitivity profiles between different cell types as well as some variability within a single type. Given that the spatial structure of the gratings experienced by the cells depend on their receptive fields and that receptive field sizes can differ substantially between cells, we analyzed to what degree this influenced the sensitivity variations within and across cell types (Fig. 5). Indeed, for both On parasol cells (Fig. 5A,B) and Off parasol cells (Fig. 5D,E), we found that the observed variability in starting and target sensitivity depended systematically on receptive field size across our recordings:

smaller cells had stronger sensitivity values and larger cells usually responded more indifferently. This makes intuitive sense, as larger receptive fields are more likely to contain both dark and bright bars of the grating for each position. For Off parasol cells, this means that cells with larger receptive fields were typically dominated by their strong sensitivity to the change of the grating position while the specific starting and target positions did not significantly influence the responses (Fig. 4A, top example). Smaller Off parasol cells, however, were also sensitive to the actual starting and target positions, which obscured the change sensitivity to some degree (Fig. 4A, bottom example).

Other aspects of the observed cell type-specific sensitivity profiles could not be explained by receptive field size. The relatively weak sensitivity to the starting position of On midget cells (Fig. 5A) as well as Off midget cells (Fig. 5D) compared with the target sensitivities of the cells (Fig. 5B,E), for example, was largely independent of receptive field size and deviated systematically from the start sensitivity of On and Off parasol cells even when receptive field sizes were similar (Fig. 5A,D). Moreover, the general weakness of change sensitivity in On cells was independent of receptive field size (Fig. 5C), and the three studied types of Off cells each displayed their respective levels of change sensitivity also largely independent of receptive field size (Fig. 5F). Note here, that the largest cells, Large Off cells, have the highest change sensitivity, and the smallest ones, Off midget cells, have the lowest change sensitivity. Yet, if larger receptive fields directly led to change sensitivity, one would expect substantial positive correlation within the individual cell types. Instead, receptive field size and change sensitivity showed either no or only a weak relationship that is not sufficient to account for cell type differences (Off midget and Large Off cells, $p > 0.05$; Off parasol cells, $R = 0.15$, $p = 0.046$). We thus conclude that change sensitivity is not simply a consequence of smaller or larger receptive fields but appears to be an intrinsic cell type-specific feature. Together, these analyses show that different types of ganglion cells systematically differ in how the combination of presaccadic and postsaccadic images affect the spiking activity during and after a saccade-like image transition.

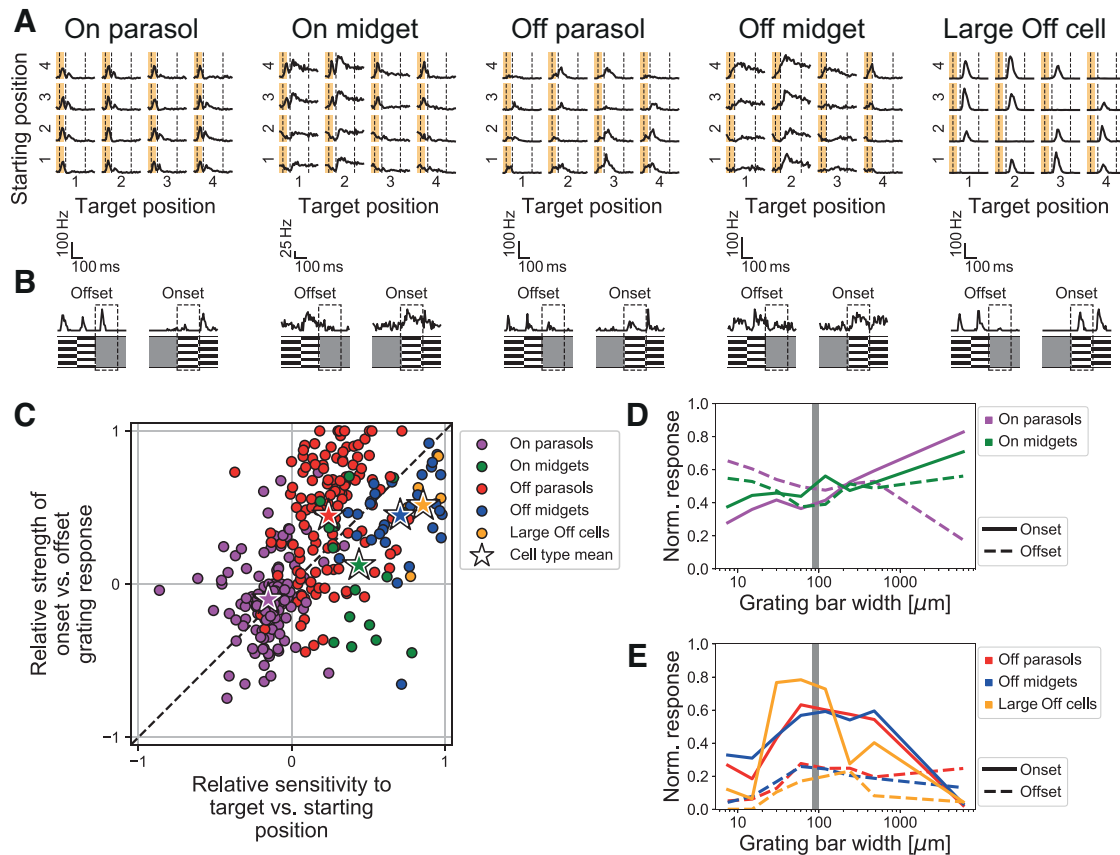


Figure 6. Comparison of saccade responses with responses to flashed gratings. **A**, Exemplary saccade responses depicted as in Figure 4A. Large Off cell is Cell 3 from Figure 1C. **B**, PSTHs of the cells in **A** in response to onset and offset of the grating stimulus. Shown is the average of the 60 and 120 μm bar width responses. The relevant part of the grating stimulus is schematically depicted beneath each PSTH. Dashed box marks the part of the response used to determine the response strength. Scale bars of **A** apply here, too. **C**, Relative strength of the response to the onset of the grating versus its offset (y -axis) and relative sensitivity to the target versus starting position during the saccadic stimulus (x -axis). Values close to 1 represent a dominant onset response/target sensitivity, values close to -1 a dominant offset response/start sensitivity. Colors denote cell types, stars represent means of the cell types. **D**, Average response strength of all On parasol/midget cells in response to the onset/offset of the grating, depending on the bar width of the grating (logarithmic axis). Response strengths are normalized to the same maximum before averaging over the cells. **E**, Same as **D** but for Off cells.

The cell type-specific differences in sensitivity to starting position versus target position raise the question whether this follows from differences in response strength under stimulus onset versus stimulus offset. For example, the relatively stronger sensitivity of a midget cell to the target position might come from stronger activation by the onset of the newly fixated target grating, whereas the offset of the previous grating (starting position) triggers little activity. We therefore compared the responses under the saccadic stimulus with responses to onsets and offsets of gratings. Since our data did not contain responses to gratings flashed individually with the same bar width and positions as in the saccadic stimulus, we instead analyzed the responses to the onset and offset of stimulation with contrast-reversing gratings. These also contained onsets and offsets at the very start and end of each reversing sequence, preceded and followed by homogeneous mean intensity illumination. Thus, for each cell, we averaged responses to the onset and offset of the reversing-gratings stimulus over bar widths of 60 and 120 μm , near the 90 μm used for the saccade stimulus, and over different spatial phases. We then compared the relative response strengths under onset versus offset, assessed as the average firing rate in the 200 ms following onset or offset, to the relative sensitivity to the target versus starting position.

From the sample cells in Figure 6, **A** and **B**, only the On parasol cell responded more strongly to the offset than the onset of the grating, which is consistent with its stronger sensitivity to the starting than to the target position. We confirmed

this observation by comparing the relative strength of the onset versus offset response with the relative sensitivity for the target versus the starting position during the saccadic stimulus for all cells (Fig. 6C). On parasol cells generally had stronger offset than onset responses and, consistent with this, had greater sensitivity for the starting compared with the target position. By contrast, responses of all Off-type cells and of the On midget cells were dominated by grating onset as well as by the sensitivity for the target position compared with sensitivity for the starting position.

We also investigated how the onset and offset response strengths of the cells depended on the grating size. The findings suggest qualitative differences between On cells (Fig. 6D) and Off cells (Fig. 6E). While Off cells responded more strongly to a grating onset than offset almost regardless of the grating size, both On parasol and On midget cells responded more strongly to the offset if the grating was sufficiently fine, but not for coarser gratings with bar widths beyond a few hundred micrometers. Thus, it seems that the relative strength of offset versus onset responses depends on the spatial stimulus structure inside the receptive field for On cells.

Note, however, that there are some caveats to these analyses of grating onsets and offsets. In particular, the small number of trials from which onset and offset responses could be gathered and the different adaptation states at onset versus offset of the reversing gratings (Appleby and Manookin, 2019; Yu et al.,

2022) contribute to variability. Furthermore, the comparison between responses to the saccade-like grating shifts and to grating onset and offset are complicated by differences in grating size and contrast.

Modeling responses to the saccadic stimulus

Given the relationship between the responses to the saccadic stimulus and the onset and offset responses to gratings, we next asked whether or to what degree the different response patterns under the saccadic stimulus followed directly from how the cells responded to simple steps in light intensity. If this was the case, the saccadic stimulus might simply be considered as a sequence of two step stimuli whose responses superimpose. Alternatively, the temporal vicinity of fixation offset and onset across a saccade could modify or add response characteristics beyond what is triggered by isolated light flashes. If so, this might hint at circuit mechanisms that are triggered specifically by saccades.

As the saccade-like motion transition of the stimulus evoked essentially the same responses as the gray transition (Fig. 1), the saccadic stimulus can be understood as a combination of an offset of bright and dark regions followed by an onset of a new bright/dark pattern. We therefore compared the responses to the saccadic stimulus with responses to full-field brightness steps from mean light intensity (gray) to high intensity (white) or to low intensity (black) and back to gray. For this stimulus, all brightness changes were temporally separated by several hundred milliseconds so that they can be considered as individual stimulation events with little influence on each other.

Under the full-field brightness steps, as expected, On cells responded to an increase in brightness, whereas Off cells responded to a decrease, and parasol cells responded more transiently than midget cells (Fig. 7A). The Large Off cells also responded transiently to decreases of the brightness, but with a longer latency than Off parasol cells.

To assess the relation between the responses to brightness steps and responses to the saccadic stimulus, we aimed at modeling the latter based on the former (Fig. 7B). Since the saccadic stimulus contains spatially structured images and given that ganglion cells can pool signals over space either linearly or nonlinearly (Enroth-Cugell and Robson, 1966; Hochstein and Shapley, 1976; Schwartz and Rieke, 2011; Gollisch, 2013; Turner and Rieke, 2016; Karamanlis and Gollisch, 2021; Zapp et al., 2022), we correspondingly set up two models with either linear or nonlinear spatial integration. The two models only differed

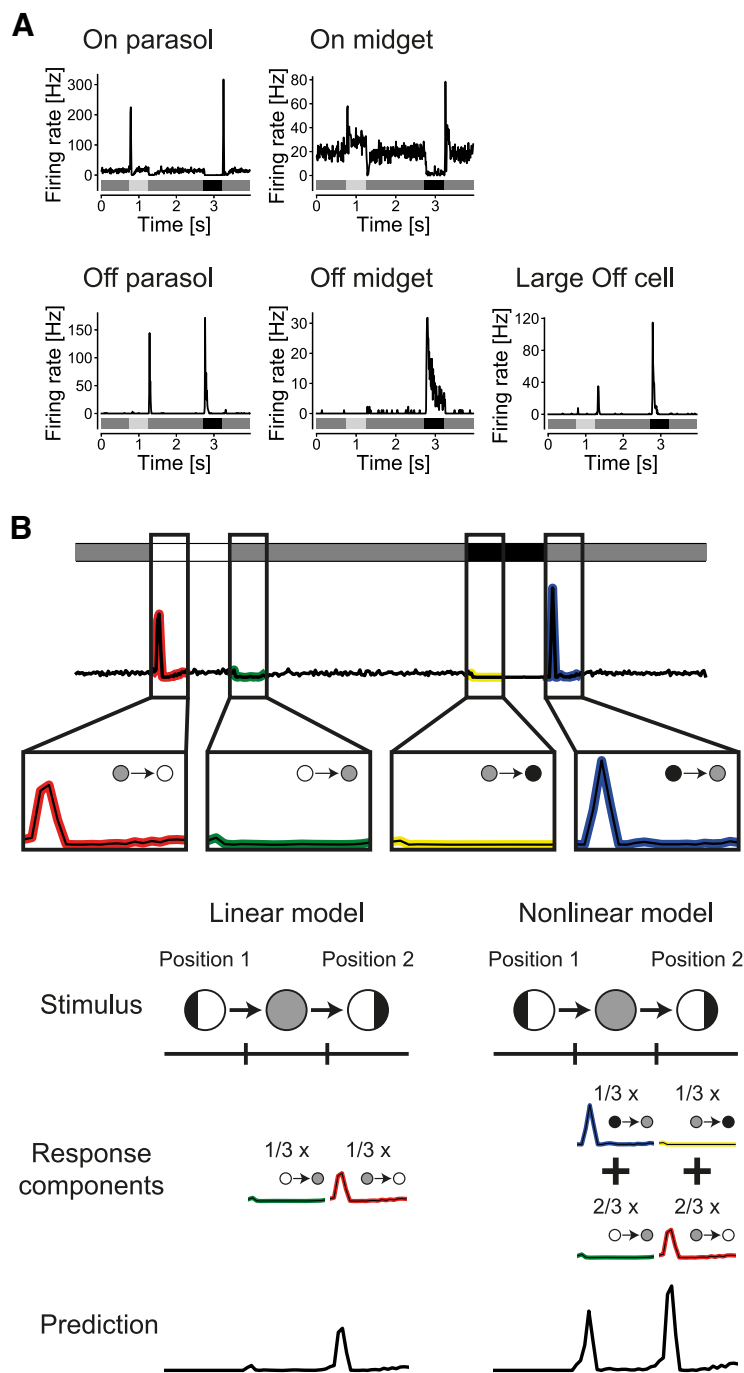


Figure 7. Modeling ganglion cell responses to saccades based on responses to brightness steps. **A**, Exemplary PSTHs for all five retinal ganglion cell types to full-field brightness steps. The stimulus is schematically depicted beneath each PSTH. **B**, Schematic depiction of obtaining a response prediction for the ON parasol cell in **A**. The response of the cell to the full-field brightness steps (top) was split into responses to the onsets and offsets of white and black (zoomed-in insets below, small circles and coloring of the PSTHs denote the brightness change). For the linear model (left), the response to an offset of the first grating was estimated by scaling the response of the cell to the offset of the appropriate brightness step, here one-third of the offset of white, corresponding to the relative decrease in mean luminance inside the receptive field. Analogously, the response to the onset of the new grating was estimated here as one-third of the onset of white, corresponding to the increase in mean brightness. Unlike what is depicted here, these two response components overlapped strongly, because of the briefness of the transition. They were then summed to form the final response prediction. For the nonlinear model (right), each pixel directly contributed response components to the final response, thereby omitting the averaging of the brightness inside the receptive field. At the offset of the first grating in this example, one-third of the receptive field turned from black to gray, and two-thirds from white to gray, yielding a one-third contribution of the black offset response and a two-thirds contribution of the white offset response. The onset of the second grating position was treated analogously and the four response components were summed to generate the final response prediction.

in the order of two simple operations: averaging signals across the receptive field and turning light intensity steps into firing rate via the measured responses to full-field brightness steps. In the spatially linear model, light intensity values of the gratings are first averaged over the receptive field, and this averaged signal is used to select and scale the appropriate responses to full-field brightness steps to obtain response predictions at fixation offset and at the subsequent new onset.

The spatially nonlinear model, on the other hand, first treats every stimulus pixel independently to select the appropriate responses to full-field brightness steps according to the brightness changes of the pixel in the saccade stimulus. These pixel contributions are then averaged across the receptive field. This averaging of the brightness-step responses incorporates local nonlinearities because—unlike in the spatially linear model—the contributions of pixels with opposite contrast do not cancel each other out. For example, the spatially nonlinear model responds to gratings even when brightening and darkening inside the receptive field are perfectly balanced because the brightness step responses to preferred and nonpreferred contrast changes are typically nonsymmetrical and therefore do not cancel. Thus, while the linear model predicts responses only according to the average brightness changes in the receptive field, the nonlinear model also includes the spatial structure of a stimulus in its response.

Note that computing the firing rate contributions on the level of individual pixels ($<10\ \mu\text{m}$ for our display) may seem counterintuitive, as this is far below the scale of bipolar cell receptive fields (Dacey et al., 2000), which are thought to correspond to the nonlinear subunits of ganglion cell receptive fields and thereby give rise to spatial nonlinearities (Demb et al., 2001; Borghuis et al., 2013; Turner and Rieke, 2016; Yu et al., 2022). Yet, because the stripes of the applied grating with a width of $90\ \mu\text{m}$ are much broader than the individual pixels, and also are similar in size or larger than expected subunits, the use of individual pixels is essentially identical to using larger subunits. For most subunits, most of the pixels experience the same sequence of light intensities and therefore contribute identical response profiles to the firing rate of a ganglion cell. For the applied grating stimulus, treating each pixel individually is thus a good approximation while avoiding the need to specify a particular subunit layout. Note also that the nonlinear model does not contain a second nonlinear step that would account for overall response transformations after spatial integration. Limiting the model to a single nonlinear stage was done for simplicity, so as to evade any parameter fits, and for keeping the complexity of the linear and the nonlinear model identical.

For both the linear and the nonlinear model, the receptive field was obtained by separating the spike-triggered average from spatiotemporal white noise stimulation (Chichilnisky, 2001) into a spatial and a temporal component and fitting a two-dimensional Gaussian to the latter. For each of the 16 transitions in the saccade stimulus, predictions were first assembled separately for the offset of the previously fixated grating and the onset of the new grating before summing the two contributions with a relative delay that corresponded to the transition time. The only two free parameters in the models were an overall scaling of response amplitude and an overall temporal shift of the predictions, which accounted for amplitude and latency differences because of differences in applied contrast. The amplitude scaling, however, did not affect our Fourier-based analysis.

For On cells, we found that the responses to the saccadic stimulus could generally be predicted well by at least one of the

two models. The responses of On parasol cells were captured well by the nonlinear model, but not by the linear model. The linear model failed, for example, to recreate the strong responses of the sample On parasol cell of Figure 8A (left) to transitions between Positions 2 and 4 (Fig. 8B). These grating positions yielded approximately equal bright and dark contrast in the receptive field of a cell (Fig. 8D), and the linear model therefore predicted no response, because these regions could cancel each other out. By contrast, the nonlinear model correctly captured the response patterns (Fig. 8C). It also succeeded in predicting a first response sensitive to the starting position and a second response sensitive to the target position, although it underestimated the strength of modulation of the second response caused by the target position.

To quantify the accuracy of the model predictions, we computed modified coefficients of determination R^2 between the response matrices of the experimental data of a cell and the response matrices as calculated from the modeled PSTHs (see Materials and Methods). For each response window, this yielded one value per cell and model, which usually lay in the range of zero (no correlation between model and data in that response window) to unity (perfect correlation between model and data). For the On parasol cells, the nonlinear model, but not the linear model, generally achieved R^2 values close to unity, especially for the first response window and only slightly less so for the second response window (Fig. 8E), corroborating the spatial nonlinearity of On parasol receptive fields under these stimulus conditions.

While the computed coefficients of determination quantify how well the amplitudes of the response peaks in the PSTHs are captured, they do not directly assess whether the models capture the sensitivity characteristics of a cell with respect to starting position, target position, and change of the grating. As an alternative measure of model accuracy, we therefore computed the distance between the measured sensitivity vector of a cell and the sensitivity vector calculated from the modeled responses. A small distance indicates that the response sensitivities have been reproduced, while a large distance represents discrepant sensitivities. For the On parasol cells, the distance of the sensitivity vectors of the linear model to the experimental sensitivity vectors was generally large, while the nonlinear model produced small distances (Fig. 8F). This confirms that On parasol responses to the saccadic stimulus could be modeled well by using the responses to a full-field stimulus and assuming a nonlinear receptive field. Only in one experiment, a subset of On parasol cells with unusually slow and weak responses to the full-field brightness step from black to gray were not modeled well by the nonlinear model.

Midget cells, like the example in Figure 8A–C (right), were modeled decently by both the linear as well as the nonlinear model. Here, the linear and the nonlinear model yielded similar response predictions because the small receptive fields of these cells contained mostly only a single bar of the grating (Fig. 8D). Because of the lack of spatial structure within the receptive field, the spatial nonlinearity played hardly any role. While the strength of the second response of the sample cell was partially overestimated, the main response properties (i.e., the transient, start-sensitive first response and the sustained, target-sensitive second response) were successfully predicted. For both response windows, the models achieved relatively high R^2 measures of the response matrices, with a tendency toward better predictions by the nonlinear model (Fig. 8E; first window, $p = 2.1 \times 10^{-5}$; second window, $p = 3.3 \times 10^{-6}$; Wilcoxon signed-rank test). The

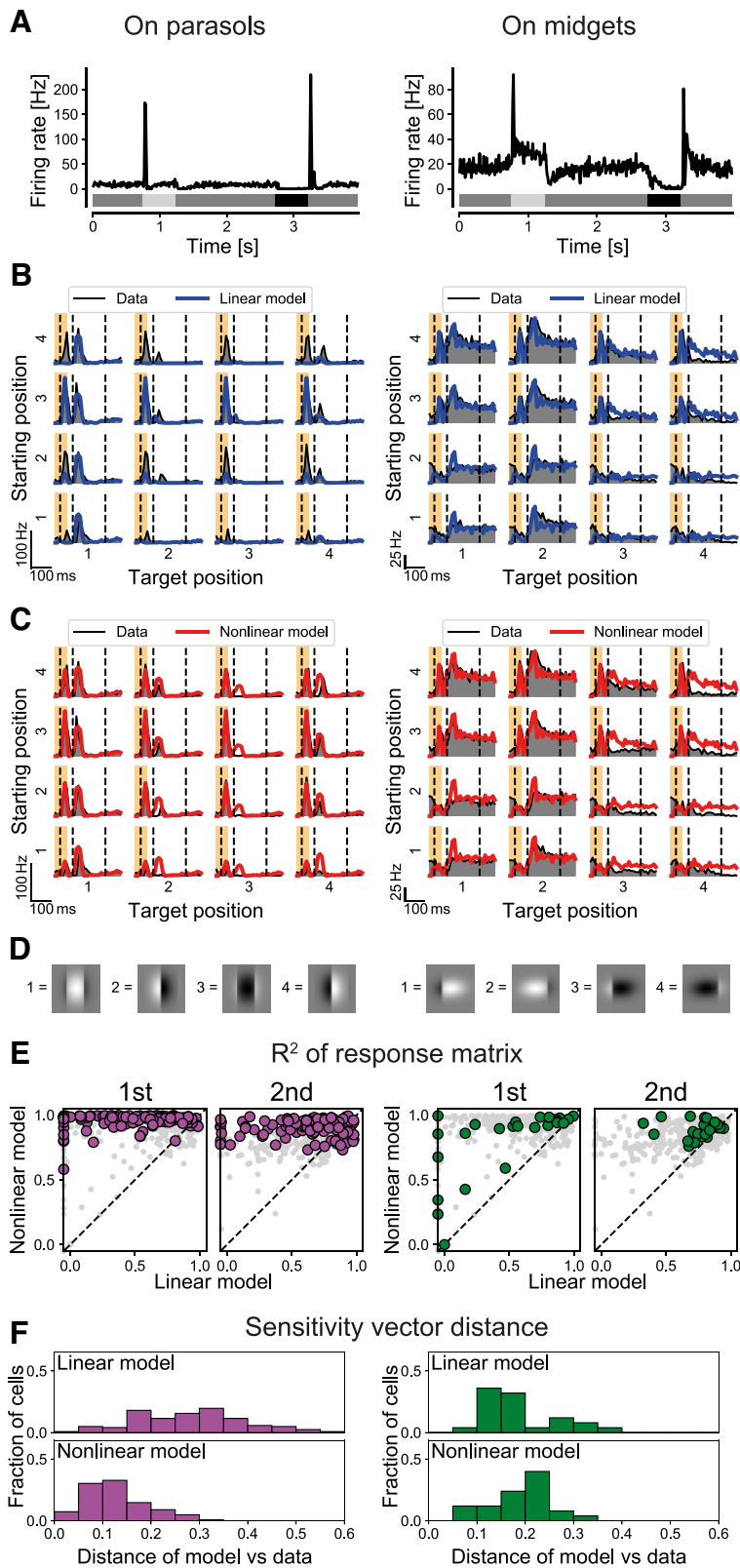


Figure 8. Model evaluation for On parasol (left) and On midget (right) cells. **A**, PSTHs of sample cells to the full-field brightness steps. The On midget cell is the same cell as in Figure 6A. **B**, Experimental responses to the saccadic stimulus (thin black line with gray filling) and predictions by the linear model (thick blue line) of the same sample cells to the saccadic stimulus. Layout of the plot is the same as in Figure 1C. **C**, Same as **B** but for the nonlinear model (red line). **D**, Illustrations of the content of the receptive fields of cells at the four grating positions. **E**, Modified coefficient of determination R^2 for the response matrix of the data versus the linear model (x-axis) and versus the nonlinear model (y-axis). R^2 values are shown separately for the first and second response matrix. Colored dots represent all ganglion cells of the cell type of the column, light gray dots all other cell types.

distance of sensitivity vectors, on the other hand, did not show a clear trend (Fig. 8F; $p = 0.21$, Wilcoxon signed-rank test).

In contrast to On cells, the responses of Off parasol cells as well as Large Off cells could only partially be explained by the linear or nonlinear model. The linear model displayed similar problems for Off parasol cells and Large Off cells as it did for On parasol cells, often strongly underestimating the responses (Fig. 9B) because of cancellation that does not occur in the nonlinear receptive fields of these cells. By contrast, the nonlinear model could mostly reproduce the sensitivities to the starting and target position (Fig. 9C). However, the responses on the diagonal (i.e., to a recurrence of the grating position) were consistently overestimated. For example, the Off parasol cell of Figure 9 lacked a strong second response to the transition when starting and target position were both Position 4. Both models predicted such a response, since the receptive field returned to being mostly filled with black after the transition (Fig. 9D). Accordingly, both the similarity between response matrices (Fig. 9E) and the sensitivity vector distance (Fig. 9F) show that the models did not capture the response characteristics of Off parasol and Large Off cells as successfully as for other cell types.

For Off midget cells, akin to On midget cells, the small size of their receptive fields led to similar predictions by the linear and nonlinear models (Fig. 9A–D, middle column). For the sample Off midget cell, the general target sensitivity was reproduced, although responses to Position 4 as target position were overestimated, possibly a result of noise in the receptive field measurement. Furthermore, the slight modulation of the responses by the starting position, hinting at some change sensitivity, was not captured by the models. For the first response window, the models achieved comparatively low R^2 values (Fig. 9E), largely because Off midget cells responded only weakly and unreliably during this window. For the second response window, however, which included the bulk of the Off midget responses, both models achieved decent R^2 values, but were likely suffering somewhat from the mild change sensitivity in the responses that was not captured by the models. The distance between the modeled and measured sensitivity vectors of the Off midget population was rather small (Fig. 9F), indicating that the general sensitivity profiles of Off midget cells could mostly be explained by their responses to the full-field brightness steps.

The analysis of Figure 5 had shown us that the receptive field size appears to directly influence

←

Cells with a model R^2 value below -0.05 have been plotted on the axis. **F**, Distributions of the distances between modeled and experimental sensitivity vectors for the linear and the nonlinear model.

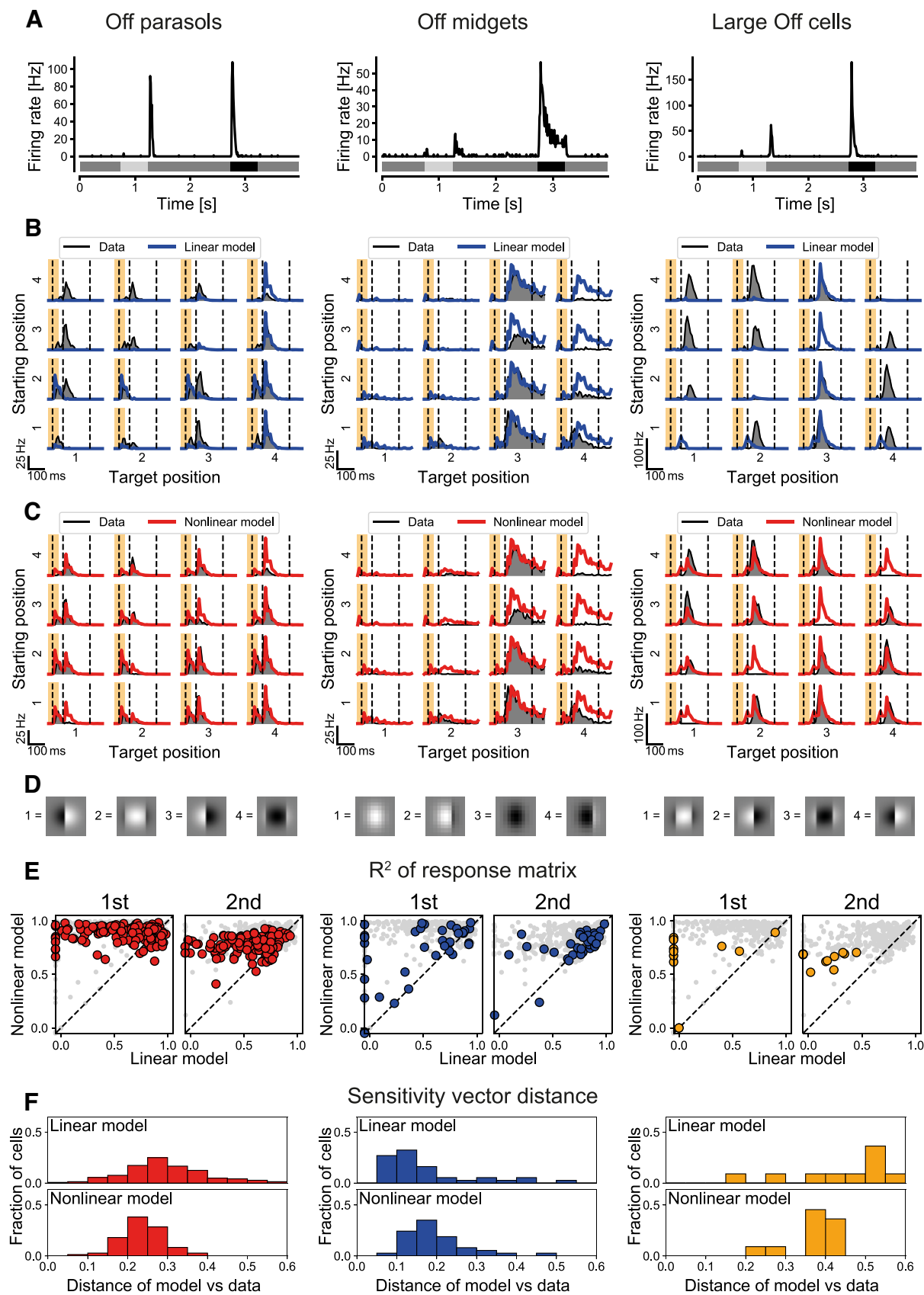


Figure 9. Model evaluation for Off cells. Same layout and subfigures as in Figure 8, but with Off parasol cells in the left column, Off midget cells in the middle column, and Large Off cells in the right column.

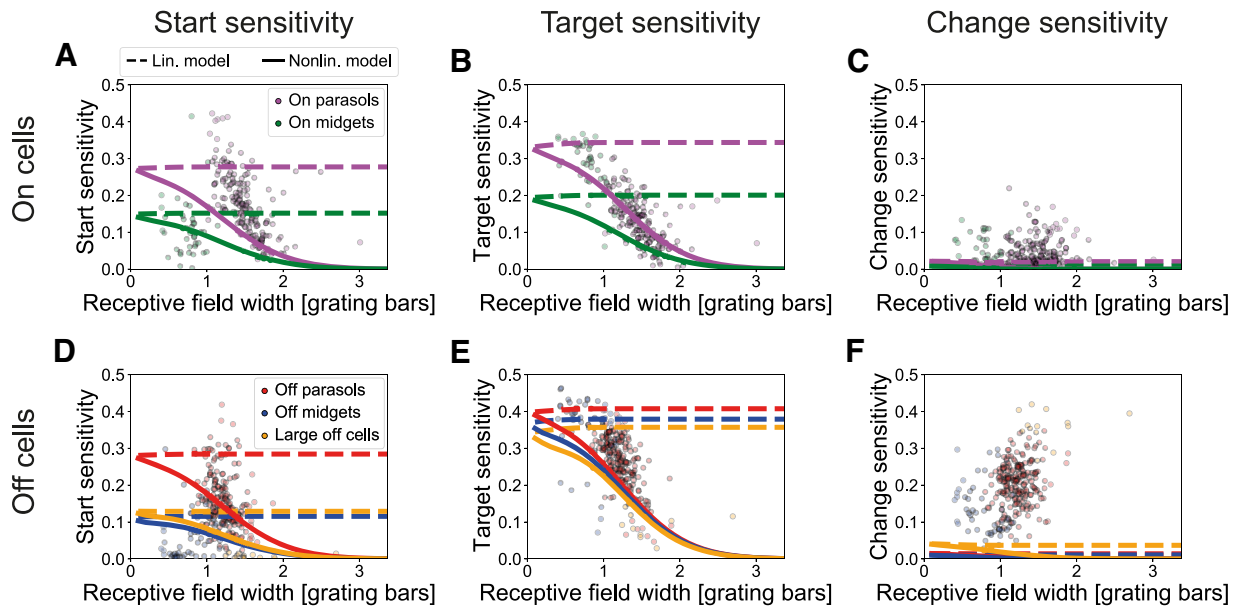


Figure 10. Influence of receptive field size on model predictions. **A**, Mean start sensitivity of each On cell type as modeled by the linear (dashed line) and nonlinear (solid line) model, depending on the receptive field width each cell was scaled to. Receptive field width was defined as in Figure 5. Measured cells are plotted in the background for reference. **B**, Same as **A**, but for target sensitivity. **C**, Same as **A**, but for change sensitivity. **D–F**, Same as **A–C**, but for Off cells.

some of the assessed sensitivities under our saccadic stimulus. We therefore used the obtained models to evaluate in simulations how the receptive field size affected the distinct response characteristics. To do so, we evaluated the response predictions by the models for each cell, with receptive fields scaled to a range of different sizes, and analyzed the resulting sensitivities, averaged over all cells of a particular type.

The sensitivities of the predictions of the linear model were independent of the receptive field size (Fig. 10, dashed lines). While the model produced weaker responses for larger receptive fields, owing to increasing cancelation from bright and dark regions inside the receptive field, the relative differences in average brightness levels of different grating positions remained and thus the preference for certain starting and target positions. In a more realistic setting, of course, the increasingly weak responses would be overshadowed by noise, thereby reducing all sensitivities.

The nonlinear model, on the other hand, directly predicted decreasing sensitivities for starting and target positions with increasing receptive field size (Fig. 10, solid lines), as the responses became more indifferent. This characteristic qualitatively matched our observations for different cell types, most notably for On and Off parasol cells. Yet, the predicted curves do not always quantitatively align with the data, and the general declining shape of all curves does not capture the fact that parasol cells, despite their larger receptive fields, were more sensitive to the starting position than midget cells. Thus, although receptive field size clearly shapes the sensitivities of the cells to starting and target position, it alone cannot explain the cell-specific preferences for starting or target position. It seems likely that, instead, the faster response kinetics of parasol cells and the strong preference of On parasol cells for offsets compared with onsets of gratings (Fig. 6) play the larger role here. Moreover, the unexplained sensitivity to change across the transition, as observed mostly for Off cells, was not predicted by any of the tested receptive field sizes (Fig. 10C,F).

Figure 11 summarizes the sensitivity measures extracted from the two models as well as from the data. Evidently, while the sensitivity to starting and target position could generally be explained

by the preference of a cell for light increments and decrements (Fig. 11A,B), in particular when using the nonlinear model, the change sensitivity could not (Fig. 11C). Accordingly, the sensitivity vectors that were calculated from the model responses were largely restricted to the plane spanned by starting and target sensitivity; the predicted change sensitivity was always close to zero (Fig. 11D, E). Therefore, the measured change sensitivity of Off parasol and Large Off cells and potentially also of Off midget cells appears to be the result of additional mechanisms. These mechanisms have the effect of spreading out the sensitivity vectors in the analyzed three-dimensional sensitivity space (Fig. 11F), thus diversifying the response characteristics of the different cell types under saccade-like image shifts.

Discussion

Saccades pose a unique challenge to the visual system by presenting a rapid transition between two fixated images, separated by less than about 100 ms. Despite their ubiquity in nearly all visual animals (Land, 1999), surprisingly little is known about how neurons in the visual system combine information from the presaccadic and postsaccadic images and what aspects of the two images are encoded in their responses in this context. In the present work, we have shown that responses of ganglion cells in the marmoset retina under saccadic stimulation do not simply represent the new fixation, but display a range of different dependencies on both the presaccadic and postsaccadic image (Fig. 1). Quantifying the sensitivity to the starting position, the target position, and change across the transition (Fig. 2) revealed that different ganglion cell types systematically displayed different sensitivity patterns (Figs. 3–5) and that some of those patterns can be related to their responses to individually flashed presaccadic and postsaccadic images (Fig. 6). Using simple models with linear and nonlinear stimulus integration over space (Fig. 7) showed that the dominant sensitivities of parasol and midget On cells could be reproduced based on the responses of the cell to isolated flashes of light intensity (Fig. 8). By contrast, for many Off cells, especially Off parasol and a class of Large Off cells, the

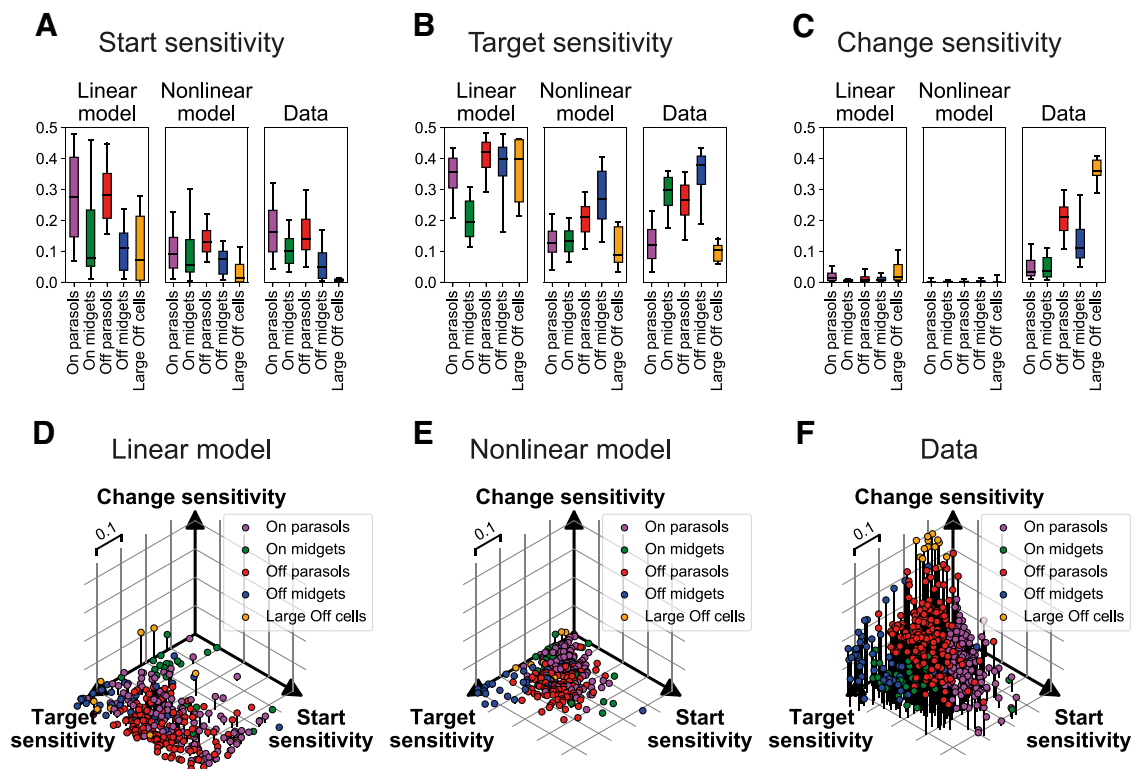


Figure 11. Sensitivity vectors from models and experiments. **A**, Boxplots for the distribution of start-sensitivity values for each cell type, obtained via each of the two models and from the experimental data. The box marks the central 50%, whiskers the central 90%, and the horizontal line inside the box the median. **B**, Same as **A**, but for target sensitivity. **C**, Same as **A** but for sensitivity to grating position change. **D**, Scatter plot of sensitivity vectors calculated from the linear model for all cells of the five types. **E**, Same as **D** but for nonlinear models. **F**, Same as **D** but for experimental data.

models failed to account for the observed sensitivity to change across the transition (Figs. 9, 10). Thus, the change sensitivity of Off cells appears to require more complex circuit mechanisms, which are not triggered under isolated light intensity flashes. This entails a new asymmetry in the functional properties of On and Off ganglion cell classes and contributes to diversifying the response patterns to saccade-like image transitions (Fig. 11).

Retinal coding of image shifts

In search of the origins of saccadic suppression, multiple studies in various nonprimate vertebrates have looked at the influence of saccades on the response strength of ganglion cells and found a diverse picture of enhancement, suppression, and indifference (Roska and Werblin, 2003; Amthor et al., 2005; Sivyer et al., 2019; Idrees et al., 2020). Fewer studies have investigated what ganglion cells encode during or after saccades, despite the likely importance of fixation onset for eliciting informative responses (Segev et al., 2007). Moreover, saccade-like image shifts may alter the message conveyed by ganglion cell spikes, as observed in the salamander retina, where On–Off ganglion cells were found to transiently switch their relative sensitivity to On-type versus Off-type stimuli after an image shift (Geffen et al., 2007). In an early study in the cat, Noda and Adey (1974) found sustained cells (probably X-cells) that responded to preferred contrast in the target image, and transient cells (probably Y-cells) that signaled the occurrence of a saccade. This is reminiscent of our findings of Off midjet cells dominated by their target sensitivity and On parasol cells with large receptive fields that responded indifferently.

In a previous study from our laboratory, we had identified ganglion cells in the mouse retina that responded distinctly to the recurrence of an image (Krishnamoorthy et al., 2017). In the

present study of the marmoset retina, we did not find such image-recurrence-sensitive cells among the investigated types. Cells with distinct responses to recurring images (Off parasol and Large Off cells) displayed decreased responses for these transitions and thus sensitivity to change rather than image recurrence. Although we cannot exclude that the primate retina also has ganglion cells with sensitivity to image recurrence, this might also reflect a divergence between mouse and primate ganglion cell types (Peng et al., 2019), demonstrating the different visual requirements of these species (Baden et al., 2020).

Relation of sensitivity profiles to basic response characteristics

Our data showed that different cell types have different relative sensitivities to the offset of the presaccadic and the onset of the postsaccadic image, as measured by the start and target sensitivity, respectively. These cell type differences seem to mostly follow the characteristics of responses to simple flash stimuli, such as temporally isolated onsets and offsets of gratings. Cell types with particularly strong responses to grating offsets, like On parasol cells, also display the highest sensitivity to the starting position, whereas cells with relatively weak grating offset responses, like Off midjet cells, were rather sensitive to the target position (Fig. 6). Furthermore, these sensitivities were approximately reproduced by computational models that were based on how the cells responded to step-like changes in light intensity (Fig. 11A,B). By contrast, the cell type differences in change sensitivity are an aspect that does not follow from simple response characteristics, as illustrated both by the finding that change sensitivity does not critically depend on receptive field size (Figs. 5F, 10F) and by the

failure of the flash response-based models to reproduce change sensitivity (Fig. 11C).

Large Off cells

In addition to the standard midget and parasol ganglion cells, we also identified a fifth cell type, which we called Large Off cells. We distinguished these cells from Off parasol cells because they had slower temporal filters and larger receptive fields, and did not match Off parasol tiling. The identity of these cells is unknown, but the similarity of their response to Off parasol cells could suggest that they might be Off smooth monostratified (Off SM) ganglion cells, though other candidates (e.g., Off narrow thorny ganglion cells) also exist (Dacey, 2004; Masri et al., 2019; Grünert and Martin, 2021). In the macaque retina, Off SM cells have been described as similar to Off parasol cells, but with a longer latency and larger receptive fields (Crook et al., 2008). In addition, SM cells tend to have irregular receptive fields with a hotspot structure (Rhoades et al., 2019), matching our observation that the Large Off cells in our recordings had more irregular receptive fields than parasol cells. Yet, we did not find the counterpart of the Off SM cells, the On SM cells, and the difference in receptive field size between Large Off and Off parasol cells was smaller than what would have been expected from Off SM cells in the macaque retina (Crook et al., 2008; Rhoades et al., 2019). The latter, however, might be a species-specific difference between macaque and marmoset or might result from differences in retinal eccentricity.

Potential mechanisms underlying responses to saccadic stimulation

The model analysis showed that the sensitivity to the starting and target position could largely be explained by the responses of a cell to full-field brightness steps, at least when nonlinear spatial integration is accounted for. Some differences between the cell types seem to follow from differences in response kinetics. The fast responses of the On parasol cells, for example, allow for a strong and distinct response to the onset of the transition with corresponding pronounced start sensitivity, whereas the slower Off midget cells respond mostly only after the new fixation has started and are thus more sensitive to the target position.

Less clear is what the mechanism behind the change sensitivity observed in Off cells, in particular Off parasol and Large Off cells, might be. One hypothesis could be that transitions with no net change in the image pattern are simply too brief to be detected by the temporal filters of the ganglion cells, particularly since we did not observe different responses for motion and gray transitions. For Off midget cells, this could potentially be a sufficient explanation, since these cells generally have slow temporal filters and their change sensitivity is only mild. For Off parasol cells, however, the temporal filters that we extracted from the spike-triggered average typically peaked far before 67 ms, which is the duration of the transition, and the change sensitivity of Large Off cells appears too stark to be caused simply by slow temporal filtering. In addition, distinct responses to the onset versus the offset of the transition are visible for all analyzed cell types except Off midget cells. Therefore, it seems unlikely that temporal filtering is so slow as to cause change sensitivity.

Alternatively, neuronal or synaptic fatigue of local excitatory inputs accrued during the fixation of several hundred milliseconds before the transition might prevent responses to the new fixation when the same image recurs. However, the pronounced transiency of responses in Off parasol and Large Off cells and the lack of sustained activity speak against strong presynaptic activity

that could trigger the required fatigue, which would need to be strong enough, for example, to prevent any response to recurring grating positions in Large Off cells.

Instead, we hypothesize that change sensitivity is caused by inhibition and propose a mechanism of local delayed crossover inhibition. In this mechanism, the Off bipolar cells that provide excitatory input to the change-sensitive Off cells receive inhibitory input (presumably onto their axon terminals) from slow, narrow-field On-type amacrine cells. For recurring grating positions, this means that the local excitation from the dark stripes of the grating at the onset of the new fixation will be suppressed by inhibition that was triggered by the brightening at the same locations when the presaccadic grating disappeared. This previously triggered inhibition will not yet have decayed, if the activity of the corresponding amacrine cell is sustained enough to last across the duration of the transition.

Crossover inhibition is the dominant inhibitory input to parasol cells and serves various functions by shaping ganglion cell responses in many species (Manookin et al., 2008; Werblin, 2010; Crook et al., 2011; Cafaro and Rieke, 2013; Rosa et al., 2016). For our hypothesized mechanism, however, we consider crossover inhibition that acts presynaptically, that is, onto bipolar cell terminals, and thereby shapes the excitatory input received by the parasol cells. This presynaptic component of crossover inhibition would act locally, suppressing only the input from certain bipolar cell locations, as required for our hypothesized mechanism of change sensitivity. Such presynaptic crossover inhibition has indeed been observed for parasol cells in the macaque retina (Crook et al., 2014; Manookin et al., 2018), as well as in other systems, such as the rabbit retina (Wässle and Boycott, 1991; Molnar and Werblin, 2007). This inhibition seems to be glycinergic (Crook et al., 2014), making glycinergic narrow-field amacrine cells with their comparatively small receptive fields (Pourcho and Goebel, 1985; Menger et al., 1998; Masland, 2012) the likely candidate source. In cat, rabbit, and rat retinas, for example, the narrow-field AII amacrine cell receives On input from bipolar cells and provides glycinergic inhibition to Off bipolar axon terminals (Kolb and Famiglietti, 1974; Demb and Singer, 2012), and a similar circuitry is also present in the macaque retina (Wässle et al., 1995).

The fact that Off parasol cells display change sensitivity, but On parasol cells do not, might then suggest that there are differences in the presynaptic crossover inhibition between these cell types. Little detail is known about these interactions, yet differences do exist. For example, blocking presynaptic inhibition unmasks a strong excitatory Off input to On parasol cells, which is not matched by corresponding inputs to Off parasol cells (Crook et al., 2014; Manookin et al., 2018). With respect to change sensitivity, one hypothesis might be that the functionally relevant difference of the presynaptic crossover inhibition lies in its timing. At the postsynaptic level of input to the ganglion cells, for example, crossover inhibition under reversing gratings is delayed with respect to excitation in Off, but not in On, parasol cells (Crook et al., 2014). If a similar timing relation occurs at the presynaptic level, the crossover inhibition from the offset of the previous fixation could be delayed enough for Off, but not On, parasol cells, to act on the onset of the new fixation and thereby suppress excitation at locations where preferred contrast recurs across the transition. When no part of the receptive field has a net increase in preferred contrast across the transition, responses of Off parasol cells would thus be diminished, whereas On cells could still respond, as the presynaptic inhibition may have already sufficiently decayed for these cells.

With respect to excitatory inputs to the ganglion cells, our efforts to model responses to the saccadic stimulus showed that spatial nonlinearities within the receptive field need to be accounted for in several cell types, in particular parasol and the Large Off cells. Rectified input from bipolar cells is the prime candidate for this (Demb et al., 2001; Borghuis et al., 2013; Turner and Rieke, 2016; Yu et al., 2022). Other mechanisms likely also contribute to shaping the responses. Gap junction coupling between bipolar cells may alter the scale of spatial nonlinearities (Kuo et al., 2016). Moreover, these gap junctions have been shown to mediate motion sensitivity in macaque parasol ganglion cells (Manookin et al., 2018; Appleby and Manookin, 2020; Liu et al., 2021) and may thus similarly modulate responses to the rapid temporal image sequence across a saccade.

Inhibition from the receptive field surround should also be triggered by the saccadic stimulus, since the gratings span the entire retina piece in the experiment, much beyond individual receptive field centers. Yet, for parasol cells, despite their spatially nonlinear receptive field center, surround suppression appears mostly mediated by horizontal cells (McMahon et al., 2004; Davenport et al., 2008), which likely do not respond strongly to the applied fine gratings because of their linear response characteristics. Moreover, given the spatial extent of the receptive field surround, it seems likely that surround suppression is similar for each of the four grating positions and therefore does not contribute to sensitivity for a particular starting or target position. Yet, in principle, surround suppression could contribute to the sensitivity to change if there are sufficiently small nonlinear subunits in the surround (Takeshita and Gollisch, 2014) or if surround inhibition acts directly on bipolar cell subunits (Protti et al., 2014). Adaptation in surround subunits, however, would rather decrease change sensitivity, as inhibition should be reduced for a recurring grating position, and thus does not present a likely mechanism for change sensitivity. Yet, future experiments might attempt to directly test for surround contributions by restricting the grating presentation to small spatial regions.

Limitations and future directions

The stimulus used here differs from real saccades in two important aspects. First, the transition is not a real motion stimulus because of the limited frame rate of our projection system. Yet, the high speed of a saccade and the corresponding motion blur make it likely that true saccadic motion and homogeneous illumination at mean light level are nearly equivalent stimuli for the retina, and we therefore do not expect this to strongly influence the findings regarding the encoding of presaccadic and postsaccadic images. Second, the applied gratings are artificial patterns, whose activation of the retinal circuitry may differ from that of natural stimuli (Turner and Rieke, 2016; Yu et al., 2022), though analyses of macaque ganglion cell responses to natural scenes containing self-motion signals found good correspondence of response characteristics with those typically obtained with simpler artificial stimuli (Schottdorf and Lee, 2021). For the present work, the periodic nature of the gratings proved useful in allowing us to apply Fourier analysis for systematically analyzing the sensitivity profile of each cell independent of the particular position of the receptive field of a cell. This may pave the way for future investigations of responses to saccades with natural images.

The use of gratings with only a single spatial scale in our recordings may raise the question of whether the analyzed sensitivity patterns differ for different spatial scales and whether some of the cell type differences follow from differences in receptive

field size among the types. The analysis of how sensitivities depend on receptive field size within cell types (Fig. 5) provides at least a partial answer. Taking advantage of the fact that receptive field sizes for individual cell types varied by a factor of ~ 2 across our data, we found that the cell type specificity of change sensitivity, for example, did not follow from differences in receptive field size. Moreover, the different types of Off cells displayed different change sensitivity even when cells of similar sizes were compared. Likewise, On midget and parasol cells differed in their start sensitivity independent of receptive field size. Nonetheless, future variations of the stimulus, including gratings with a smaller or larger spatial frequency, would be useful to study the generality of our findings. For example, probing the small midget cells with stimuli that contain substantial spatial structure in their receptive fields might elucidate whether Off midget cells robustly display some level of change sensitivity or whether their responses simply deteriorate at higher spatial frequency.

Regarding our analysis approach, we note that the response patterns elicited by the saccadic stimulus could contain an additional structure that is not captured by our separation into two response windows and analysis of peak firing rates. The two applied response windows make intuitive sense, however, as they relate to the offset and onset of fixated images, and many cells indeed displayed distinct response peaks in the two time windows, in particular On parasol cells, but also Off parasol and On midget cells. As these peaks were similar in timing across types within a given piece of retina, it allowed us to use a single boundary to separate these response components. For Off midget cells, this separation is less clear, as responses were more sustained without distinct peaks and had only a little activity in the first response window. Thus, one might ask whether a potential offset response might come later and overlap with the subsequent onset response.

But Off midget cells generally did not show any sizeable offset-triggered response that would be invariant to the target position (Fig. 4, see the two sample Off midget cells, in particular for the 2-to-2 transition in the top row and the 4-to-4 transition below, which both have the preferred starting position). Thus, responses of Off midget cells are not consistent with containing a strong offset-specific (and target-invariant) response component that would be mixed with the onset component; instead, the particular starting position can modulate the response that is triggered by the preferred target position, which is what is captured in our analysis as change sensitivity.

Future experiments might probe the time scales of the response components and their interactions further by varying the duration of the transition period. This might help reveal, for example, the timescale of the change sensitivity and relate this to potential inhibitory mechanisms. Finally, to test whether cross-over inhibition is involved in generating the change-sensitive responses of Off cells, blocking the On pathway with L-AP-4 (Slaughter and Miller, 1981) could be applied to remove On-type inhibition, although this would not reveal specifics of the potential crossover circuitry.

Asymmetry of the On and Off pathways

The On and Off pathways in the retina had originally been viewed as symmetrical (i.e., exhibiting the same response properties but for light increments and decrements, respectively; Schiller, 1992). Later, however, several studies found asymmetries between the On and Off pathways, such as differences in the

spatiotemporal receptive field properties of macaque On and Off parasol ganglion cells (Chichilnisky and Kalmar, 2002). These differences might be linked to different connectivity in the underlying circuitry of the On and Off pathways found in primates and other species (Molnar and Werblin, 2007; Khuc-Trong and Rieke, 2008) and to the more strongly rectified synaptic input received by primate Off parasol cells (but also, e.g., guinea pig Off Y-cells) compared with their On counterparts (Zaghloul et al., 2003; Turner and Rieke, 2016). Importantly, these asymmetries extend to relevant functional differences like the encoding of natural images (Turner and Rieke, 2016).

While asymmetries between On and Off parasol cells (or Y-cells in other species) have been described previously, the midget pathways have received less attention. In the present work, we found asymmetries between the On and Off pathways of both parasol as well as midget ganglion cells. While Off midget cells were strongly sensitive to the target image with some change sensitivity, On midget cells were not change sensitive, but responded transiently to the preferred starting image. The asymmetrical responses of parasol cells were even more striking. While On parasol responses represented images before and after a transition successively, Off parasol cells performed a computation across the transition by responding specifically to a change of the image. The different response characteristics suggest that On and Off cells encode different features of the visual stimulus in the context of saccades, similar to recent suggestions about the functional benefit of differences in spatial integration between On and Off parasol cells (Yu et al., 2022). This may allow the joint activity patterns of On and Off pathways to cover a more versatile stimulus space at the onset of a new fixation than pathways with similar sensitivity profiles, but opposing contrast sensitivity.

References

- Amthor FR, Tootle JS, Gawne TJ (2005) Retinal ganglion cell coding in simulated active vision. *Vis Neurosci* 22:789–806.
- Appleby TR, Manookin MB (2019) Neural sensitization improves encoding fidelity in the primate retina. *Nat Commun* 10:4017.
- Appleby TR, Manookin MB (2020) Selectivity to approaching motion in retinal inputs to the dorsal visual pathway. *eLife* 9:e51144.
- Baden T, Euler T, Berens P (2020) Understanding the retinal basis of vision across species. *Nat Rev Neurosci* 21:5–20.
- Borghuis BG, Marvin JS, Looger LL, Demb JB (2013) Two-photon imaging of nonlinear glutamate release dynamics at bipolar cell synapses in the mouse retina. *J Neurosci* 33:10972–10985.
- Cafaro J, Rieke F (2013) Regulation of spatial selectivity by crossover inhibition. *J Neurosci* 33:6310–6320.
- Chichilnisky EJ (2001) A simple white noise analysis of neuronal light responses. *Network* 12:199–213.
- Chichilnisky EJ, Kalmar RS (2002) Functional asymmetries in ON and OFF ganglion cells of primate retina. *J Neurosci* 22:2737–2747.
- Crook JD, Peterson BB, Packer OS, Robinson FR, Gamlin PD, Troy JB, Dacey DM (2008) The smooth monostriated ganglion cell: evidence for spatial diversity in the Y-cell pathway to the lateral geniculate nucleus and superior colliculus in the macaque monkey. *J Neurosci* 28:12654–12671.
- Crook JD, Manookin MB, Packer OS, Dacey DM (2011) Horizontal cell feedback without cone type-selective inhibition mediates “red–green” color opponency in midget ganglion cells of the primate retina. *J Neurosci* 31:1762–1772.
- Crook JD, Packer OS, Dacey DM (2014) A synaptic signature for ON- and OFF-center parasol ganglion cells of the primate retina. *Vis Neurosci* 31:57–84.
- Dacey D, Packer OS, Diller L, Brainard D, Peterson B, Lee B (2000) Center surround receptive field structure of cone bipolar cells in primate retina. *Vision Res* 40:1801–1811.
- Dacey DM (2004) Origins of perception: retinal ganglion cell diversity and the creation of parallel visual pathways. In: *The cognitive neurosciences* (Gazzaniga MS, ed), pp 281–301. Cambridge, MA: MIT.
- Davenport CM, Detwiler PB, Dacey DM (2008) Effects of pH buffering on horizontal and ganglion cell light responses in primate retina: evidence for the proton hypothesis of surround formation. *J Neurosci* 28:456–464.
- Demb JB, Singer JH (2012) Intrinsic properties and functional circuitry of the AII amacrine cell. *Vis Neurosci* 29:51–60.
- Demb JB, Zaghloul K, Haarsma L, Sterling P (2001) Bipolar cells contribute to nonlinear spatial summation in the brisk-transient (Y) ganglion cell in mammalian retina. *J Neurosci* 21:7447–7454.
- Enroth-Cugell C, Robson JG (1966) The contrast sensitivity of retinal ganglion cells of the cat. *J Physiol* 187:517–552.
- Field GD, Sher A, Gauthier JL, Greschner M, Shlens J, Litke AM, Chichilnisky EJ (2007) Spatial properties and functional organization of small bistratified ganglion cells in primate retina. *J Neurosci* 27:13261–13272.
- Gaveau V, Martin O, Prablanc C, Pélisson D, Urquizar C, Desmurget M (2003) On-line modification of saccadic eye movements by retinal signals. *Neuroreport* 14:875–878.
- Geffen MN, de Vries SEJ, Meister M (2007) Retinal ganglion cells can rapidly change polarity from Off to On. *PLoS Biol* 5:e65.
- Gollisch T (2013) Features and functions of nonlinear spatial integration by retinal ganglion cells. *J Physiol Paris* 107:338–348.
- Gomes FL, Silveira LCL, Saito CA, Yamada ES (2005) Density, proportion, and dendritic coverage of retinal ganglion cells of the common marmoset (*Callithrix jacchus jacchus*). *Braz J Med Biol Res* 38:915–924.
- Grünert U, Martin PR (2021) Morphology, molecular characterization, and connections of ganglion cells in primate retina. *Annu Rev Vis Sci* 7:73–103.
- Hartline HK (1938) The response of single optic nerve fibers of the vertebrate eye to illumination of the retina. *Am J Physiol* 121:400–415.
- Hochstein S, Shapley RM (1976) Linear and nonlinear spatial subunits in Y cat retinal ganglion cells. *J Physiol* 262:265–284.
- Idrees S, Baumann MP, Franke F, Münch TA, Hafed ZM (2020) Perceptual saccadic suppression starts in the retina. *Nat Commun* 11:1977.
- Karamanlis D, Gollisch T (2021) Nonlinear spatial integration underlies the diversity of retinal ganglion cell responses to natural images. *J Neurosci* 41:3479–3498.
- Karamanlis D, Schreyer HM, Gollisch T (2022) Retinal encoding of natural scenes. *Annu Rev Vis Sci* 8:171–193.
- Khuc-Trong P, Rieke F (2008) Origin of correlated activity between parasol retinal ganglion cells. *Nat Neurosci* 11:1343–1351.
- Kolb H, Famiglietti EV (1974) Rod and cone pathways in the inner plexiform layer of cat retina. *Science* 186:47–49.
- Krishnamoorthy V, Weick M, Gollisch T (2017) Sensitivity to image recurrence across eye-movement-like image transitions through local serial inhibition in the retina. *eLife* 6:e22431.
- Kuo SP, Schwartz GW, Rieke F (2016) Nonlinear spatiotemporal integration by electrical and chemical synapses in the retina. *Neuron* 90:320–332.
- Lamb TD (1995) Photoreceptor spectral sensitivities: common shape in the long-wavelength region. *Vision Res* 35:3083–3091.
- Land MF (1999) Motion and vision: why animals move their eyes. *J Comp Physiol A* 185:341–352.
- Lettvin JY, Maturana HR, McCulloch WS, Pitts WH (1959) What the frog’s eye tells the frog’s brain. *Proc IRE* 47:1940–1951.
- Liu B, Hong A, Rieke F, Manookin MB (2021) Predictive encoding of motion begins in the primate retina. *Nat Neurosci* 24:1280–1291.
- Manookin MB, Beaudoin DL, Ernst ZR, Flagel LJ, Demb JB (2008) Disinhibition combines with excitation to extend the operating range of the OFF visual pathway in daylight. *J Neurosci* 28:4136–4150.
- Manookin MB, Patterson SS, Linehan CM (2018) Neural mechanisms mediating motion sensitivity in parasol ganglion cells of the primate retina. *Neuron* 97:1327–1340.e4.
- Masland RH (2012) The tasks of amacrine cells. *Vis Neurosci* 29:3–9.
- Masri RA, Percival KA, Koizumi A, Martin PR, Grünert U (2019) Survey of retinal ganglion cell morphology in marmoset. *J Comp Neurol* 527:236–258.
- McMahon MJ, Packer OS, Dacey DM (2004) The classical receptive field surround of primate parasol ganglion cells is mediated primarily by a non-GABAergic pathway. *J Neurosci* 24:3736–3745.

- Menger N, Pow DV, Wässle H (1998) Glycinergic amacrine cells of the rat retina. *J Comp Neurol* 401:34–46.
- Molnar A, Werblin F (2007) Inhibitory feedback shapes bipolar cell responses in the rabbit retina. *J Neurophysiol* 98:3423–3435.
- Noda H, Adey WR (1974) Retinal ganglion cells of the cat transfer information on saccadic eye movement and quick target motion. *Brain Res* 70:340–345.
- Pachitariu M, Steinmetz NA, Kadir SN, Carandini M, Harris KD (2016) Fast and accurate spike sorting of high-channel count probes with KiloSort. *Adv Neural Inf Process Syst* 29:4448–4456.
- Peng Y-R, Shekhar K, Yan W, Herrmann D, Sappington A, Bryman GS, van Zyl T, Do MTH, Regev A, Sanes JR (2019) Molecular classification and comparative taxonomics of foveal and peripheral cells in primate retina. *Cell* 176:1222–1237.e22.
- Pourcho RG, Goebel DJ (1985) A combined Golgi and autoradiographic study of (³H)glycine-accumulating amacrine cells in the cat retina. *J Comp Neurol* 233:473–480.
- Protti DA, Di Marco S, Huang JY, Vonhoff CR, Nguyen V, Solomon SG (2014) Inner retinal inhibition shapes the receptive field of retinal ganglion cells in primate. *J Physiol* 592:49–65.
- Rhoades CE, Shah NP, Manookin MB, Brackbill N, Kling A, Goetz G, Sher A, Litke AM, Chichilnisky EJ (2019) Unusual physiological properties of smooth monostratified ganglion cell types in primate retina. *Neuron* 103:658–672.e6.
- Rosa JM, Ruehle S, Ding H, Lagnado L (2016) Crossover inhibition generates sustained visual responses in the inner retina. *Neuron* 90:308–319.
- Roska B, Werblin F (2003) Rapid global shifts in natural scenes block spiking in specific ganglion cell types. *Nat Neurosci* 6:600–608.
- Schiller PH (1992) The ON and OFF channels of the visual system. *Trends Neurosci* 15:86–92.
- Schnapf JL, Nunn BJ, Meister M, Baylor DA (1990) Visual transduction in cones of the monkey macaca fascicularis. *J Physiol* 427:681–713.
- Schneeweis DM, Schnapf JL (1995) Photovoltage of rods and cones in the macaque retina. *Science* 268:1053–1056.
- Schottdorf M, Lee BB (2021) A quantitative description of macaque ganglion cell responses to natural scenes: the interplay of time and space. *J Physiol* 599:3169–3193.
- Schwartz G, Rieke F (2011) Nonlinear spatial encoding by retinal ganglion cells: when $1 + 1 \neq 2$. *J Gen Physiol* 138:283–290.
- Segev R, Schneidman E, Goodhouse J, Berry MJ (2007) Role of eye movements in the retinal code for a size discrimination task. *J Neurophysiol* 98:1380–1391.
- Sivyer B, Tomlinson A, Taylor WR (2019) Simulated saccadic stimuli suppress ON-type direction-selective retinal ganglion cells via glycinergic inhibition. *J Neurosci* 39:4312–4322.
- Slaughter MM, Miller RF (1981) 2-amino-4-phosphonobutyric acid: a new pharmacological tool for retina research. *Science* 211:182–185.
- Takeshita D, Gollisch T (2014) Nonlinear spatial integration in the receptive field surround of retinal ganglion cells. *J Neurosci* 34:7548–7561.
- Tovée MJ, Bowmaker JK, Mollon JD (1992) The relationship between cone pigments and behavioural sensitivity in a new world monkey (*Callithrix jacchus jacchus*). *Vision Res* 32:867–878.
- Travis DS, Bowmaker JK, Mollon JD (1988) Polymorphism of visual pigments in a callitrichid monkey. *Vision Res* 28:481–490.
- Troilo D, Howland HC, Judge SJ (1993) Visual optics and retinal cone topography in the common marmoset (*Callithrix jacchus*). *Vision Res* 33:1301–1310.
- Turner MH, Rieke F (2016) Synaptic rectification controls nonlinear spatial integration of natural visual inputs. *Neuron* 90:1257–1271.
- Wässle H, Boycott BB (1991) Functional architecture of the mammalian retina. *Physiol Rev* 71:447–480.
- Wässle H, Grünert U, Chun M-H, Boycott BB (1995) The rod pathway of the macaque monkey retina: identification of AII-amacrine cells with antibodies against calretinin. *J Comp Neurol* 361:537–551.
- Werblin FS (2010) Six different roles for crossover inhibition in the retina: correcting the nonlinearities of synaptic transmission. *Vis Neurosci* 27:1–8.
- Wienbar S, Schwartz GW (2018) The dynamic receptive fields of retinal ganglion cells. *Prog Retin Eye Res* 67:102–117.
- Wurtz RH (2008) Neuronal mechanisms of visual stability. *Vision Res* 48:2070–2089.
- Yarbus AL (1967) Eye movements and vision. New York: Plenum.
- Yu Z, Turner MH, Baudin J, Rieke F (2022) Adaptation in cone photoreceptors contributes to an unexpected insensitivity of primate On parasol retinal ganglion cells to spatial structure in natural images. *eLife* 11:e70611.
- Zaghloul KA, Boahen K, Demb JB (2003) Different circuits for ON and OFF retinal ganglion cells cause different contrast sensitivities. *J Neurosci* 23:2645–2654.
- Zapp SJ, Nitsche S, Gollisch T (2022) Retinal receptive-field substructure: scaffolding for coding and computation. *Trends Neurosci* 45:430–445.